REFERENCES

Beyer, F.L., Tan, N.C., Dasgupta, A., and Galvin, M.E. (2002). Polymer-layered silicate nanocomposites from model surfactants. Chemistry Materials, 14, 2983-2988.

Biswas, M. and Sinharay, S. (1997). Preparation and evaluation of composites from montmorillonite and some heterocyclic polymers. 1: poly(N-vinylcarbazole)-montmorillonite nanocomposite system. Polymer, 39(25), 6423-6428.

Bhat, N.V., Geetha, P., Pawde, S., and Nallathambi, R. (1995). Preparation of poly(vinylidine fluoride)- polypyrrole composite films by electrochemical synthesis and their properties. Journal of Applied Polymer Science, 58, 2251-2257.

Chen, J.H., Huang, Z.P., Wang, D.Z., Yang, S.X., Li, W.Z., Wen, J.G., and Ren, Z.F. (2002). Electrochemical synthesis of polypyrrole films over each of well-aligned carbon nanotubes. Synthetic Metals, 125, 289-294.

Giannelis, E.P. (1996). Polymer layered silicate nanocomposites. Advanced Materials, 8(1), 29-35.

Hong, S.H., Kim, B.H., Joo, J., Kim, J.W., and Choi, H.J. (2001). Polypyrrole-montmorillonite nanocomposites synthesized by emulsion polymerization. Current Applied Physics, 1, 447-450.

Jesus, M.C., Weiss, R.A., and Hahn, S.F. (1998). Synthesis of conductive nanocomposites by selective in situ polymerization of pyrrole within the lamellar microdomains of a block copolymer. Macromolecules, 31, 2230-2235.

Kang, E.T., Neoh, K.G., and Tan, K.L, *Advances in Polymer Science 106 Polymer Characteristics*, (pp. 135-190). Berlin: Springer-Verlag (1993).

Kim, B.H., Jung, J.H., Kim, J.W., Choi, H.J., and Joo, J. (2001). Physical characterization of polyaniline-Na^+-montmorillonite nanocomposite intercarlated by emulsion polymerization. Synthetic Metals, 117, 115-118.

Kim, J.W., Liu, F., Choi, H.J., Hong, S.H., and Joo, J. (2003). Intercalated polypyrrole/Na^{+}-montmorillonite nanocomposite via an inverted emulsion pathway method. Polymer, 44, 289-293.

Kim, S.R., Choi, S.A., Kim, J.D., Kim, K.J., Lee, C., and Rhee, S.B. (1995). Preparation of polythiophene LB films and their gas sensitivities by the quartz crystal microbalance. Synthetic Metals, 71, 2027-2028.

Liang, L., Liu, J., and Gong, X. (2000). Thermosensitive poly(N-isopropylacrylamide)-clay nanocomposites with enhanced temperature response. Langmuir, 16, 9895-9899.

Liu, Y.C. and Tsai, C.J. (2003). Enhancements in conductivity and thermal and conductive stabilities of electropolymerized polypyrrole with caprolactam-modified clay. Chemistry Materials, 15, 320-326.

Magaraphan, R., Lilayuthalert, W., Siriwat, A., and Schwank, J.W. (2001). Preparation, structure, properties and thermal behavior of rigid-rod polyimide/montmorillonite nanocomposites. Composites Science and Technology, 61, 1253-1264.

Messersmith, P.B. and Guannelis, E.P. (1995). Synthesis and barrier properties of poly(ε-caprolactone)-layered silicate nanocomposites. Journal of Polymer Science: Part A: Polymer Chemistry, 33, 1047-1057.

Moon, G.H. and Seung, S.I. (1999). Electrical and structural analysis of conductive polyaniline/polyimide blends. Journal of Applied Polymer Science, 71, 2169-2178.

Nascimento, G.M., Constantino, V.R.L., and Tempirini, M.L.A. (2002). Spectroscopic characterization of a new type of conducting polymer-clay nanocomposite. Macromolecules, 35, 7535-7537.

Omastowa, M., Pavlinec, J., Pionteck, J., Simon, F., and Konisa, S. (1997). Chemical preparation and characterization of conductive poly(metyl methacrylate)/polypyrrole composites. Polymer, 39(25), 6559-6566.

Pinnavaia, T.J. and Beall, G.W. (2000). Polymer-clay Nanocomposites. (pp. 97-149). London: John Wiley & Sons Ltd.

Ramelow, U., Ma, J.H., and Darbeau, R. (2001). Electrical conductivies of polypyrrole reacted with dopant solutions. Material Resolution Innovat. 5, 40-49.

Ratanarat, K., Nithitanakul, M., Martin, D.C., and Magaraphan, M. (2003). Polymer-layered Silicate Nanocomposites in Solution: Linear PEO and Highly Branched Dendrimer for Organic Wastewater Treatment. Reviews on Advanced Materials Science, 5(3), 187-192.

Sinharay, S. and Biswas, M. (1999). Preparation and evaluation of composites from montmorillonite and some heterocyclic polymers: 3. a water dispersible nanocomposite from pyrrole-montmorillonite polymerization system. Materials Research Bulletin, 34(8), 1187-1194.

Selampinar, F., Levent T., Ural, A., Talat, Y., and Sesik, S. (1995). A conducting composite of polypyrrole II. as a gas sensor. Synthetic Metals, 68, 109-116.

Selampinar, F., Ural, A., Tulay, Y., Attila, G., and Levent, T. (1997). Synthesis of a hexafluoropropylidene-bis(phthalic anhydride)-based polyimide and its conducting polymer composites with polypyrrole. Journal of Polymer Science: Part A: Polymer Chemistry, 35, 3009-3016.

Sinharay, S. and Okamoto, M. (2003). Polymer/layered silicate nanocomposites: a review from preparation to processing. Progress in Polymer Science, 28, 1539-1641.

Thaijaroen, W. (2000). Preparation and Mechanical Properties of NR/clay Nanocomposites. M.S. Thesis in Polymer Science, Petroleum and Petrochemical College, Chulalongkorn University.

Tyan, H.L., Liu, Y.C., and Wei, K.H. (1999). Thermally and mechanically enhanced clay/polyimide nanocomposite via reactive organoclay. Chemistry Materials, 11, 1942-1947.

Wallace, G.G., Spinks, G.M., Kane-Maguire, L.A.P., and Teasdale, P.R. (2003). Conductive Electroactive Polymers. (pp. 51-119) New York: CRC Press LLC.

Wu, Q., Xue, Z., Qi, Z., and Wang, F. (2000). Synthesis and characterization of PAn/clay nanocomposite with extended chain conformation of polyaniline. Polymer, 41, 2029-2032.

Yeh, J.M., Liou, S.J., Lai, C.Y., and Wu, P.C. (2001). Enhancement of corrosion protection effect in polyaniline via the formation of polyaniline-clay nanocomposite materials. Chemistry Materials, 13, 1131-1136.

Zhu, J., Morgan, A.B., Lamelas, F.J., and Wilkie, C.A. (2001). Fire properties of polystyrene-clay nanocomposites. Chemistry Materials, 13, 3774-3780.

APPENDICES

Appendix A Characterization of organically modified MMT

After modification of Na-MMT, sodium ions in the galleries of MMT were replaced by the quarternary ammonium ions of octadecylammine, a modifying agent, and the organically modified MMT (OC-MMT) was characterized by using FT-IR, XRD, and TGA.

FTIR

FTIR could be used for verifying the incorporation of a modifying agent into the galleries of MMT. Figure A1 showed the FT-IR spectra of a modifying agent, Na-MMT, and the organically modified MMT.

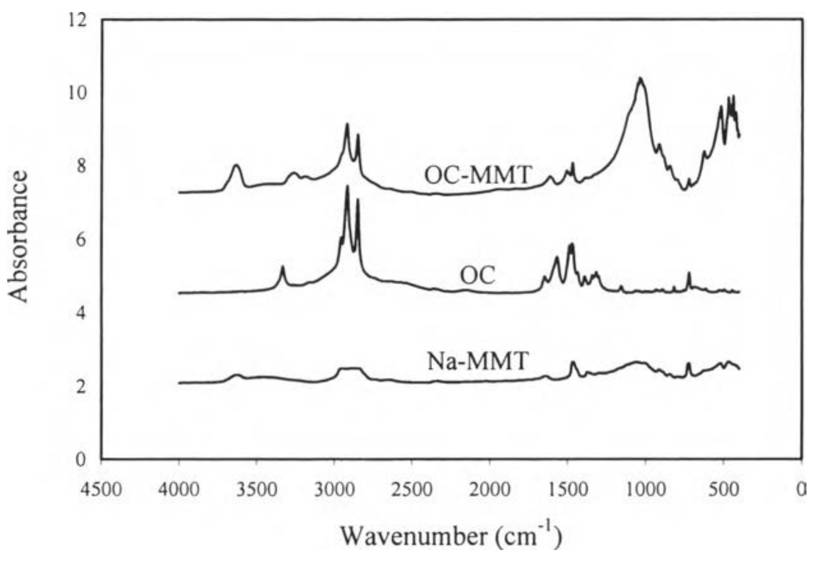

Figure A1 FTIR spectra of Na-MMT, OC, and OC-MMT.

As shown in Figure A1, octadecylamine (OC) showed the important absorption peaks of N-H stretching, C-H stretching of methyl and methylene group at 3300, 2950, 2850 and 1430 cm^{-1}, respectively. For the organically modified MMT obtained, the FT-IR spectra showed the combination between the characteristic peaks of inorganic Na-MMT and octadecylamine.

XRD

Besides FT-IR, XRD also provided strong evidence for the incorporation of a modifying agent into the MMT structure as well. The XRD analysis of Na-MMT and the organically modified MMT prepared using octadecylamine as a modifying agent were shown in Figure A2. There was some little amount of Na-MMT or the retraction of MMT remaining in the modified OC-MMT as seen by the small peak at 2 Theta = 7.9 degrees.

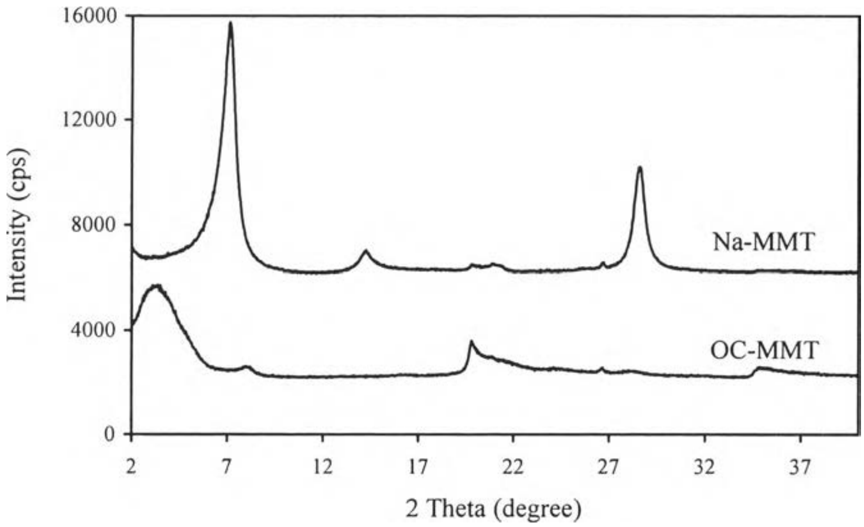

Figure A2 XRD patterns of Na-MMT, and OC-MMT.

From Figure A2, the peak position below 10-degree of 2 Theta of OC-MMT was shifted to lower degree relative to that of Na-MMT, suggesting that the spaces between the silicate layers were significantly expanded. This is due to the incorporation of a modifying agent into the galleries of MMT. The basal spacing calculated from the peak position of 2 Theta (degree) was listed in Table A1.

Table A1 The basal spacing of Na-MMT, and OC-MMT.

MMT	Basal spacing (Å)
Na-MMT	12.41
OC-MMT	26.12

The results from XRD revealed that the basal spacing of Na-MMT obtained from this work was 12.41 Å (7.12 degree) which was slightly different from Thaijaroen (2000), 12.13 Å. After modifying with octadecylamine, the basal spacing of OC-MMT was to be 26.12 Å (3.38 degree); however, there were some remained Na-MMT whose basal spacing of silicate layer retracted to 11.44 Å (7.72 degree) which was closed to that reported by Giannelis *et al.* (1996), 11.40 Å. The higher degree of basal spacing expansion generally results in the higher opportunity of polymer intercalation, leading to the more possibility of layered-silicate deamination in polymer matrix.

TGA

The incorporation of a modifying agent into the galleries of MMT was also determined by using Thermogravemetric analysis. TGA curves of a modifying agent, Na-MMT and the organically modified MMT under N_2 atmosphere up to 800°C were shown in Figure A3.

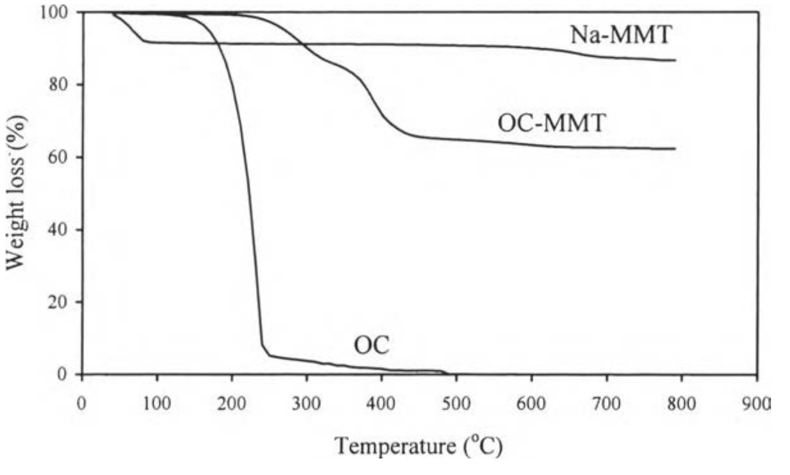

Figure A3 TGA curves of OC, Na-MMT, and OC-MMT.

As shown in Figure 4.3, the degradation temperature (T_d) obtained by derivative of OC was observed at about 180°C while that of Na-MMT was about 630°C. For OC-MMT, the obvious degradation temperature was around 373°C. This could confirm the improvement in thermal stability of a modifying agent incorporated in the galleries of MMT structure

Appendix B Response time to CO_2, CH_4 and C_2H_4 at room temperature for all of the sensor samples

Table B1 Response time to CO_2 at room temperature for all of the sensor samples at various thicknesss.

Samples	Response time (sec)		
	Thickness (mm)		
	0.5	0.8	1.0
PPy	100	130	140
PPyC1	90	110	120
PPyC3	90	120	130
PPyC6	90	100	150
PPyC9	100	120	140
DPPyC3	100	110	140
nDPPyC3	100	-	-

Table B2 Response time to CH_4 at room temperature for all of the sensor samples at various thickness.

Samples	Response time (sec)		
	Thickness (mm)		
	0.5	0.8	1.0
PPy	90	120	150
PPyC1	80	90	130
PPyC3	80	90	150
PPyC6	80	90	150
PPyC9	80	100	130
DPPyC3	70	90	110
nDPPyC3	100	-	-

Table B3 Response time to C_2H_4 at room temperature for all of the sensor samples at various thickness.

Samples	Response time (sec)		
	Thickness (mm)		
	0.5	0.8	1.0
PPy	90	100	120
PPyC1	80	90	100
PPyC3	70	80	90
PPyC6	60	100	120
PPyC9	60	110	120
DPPyC3	60	70	100
nDPPyC3	100	-	-

Table B4 Response time to CO_2, CH_4 and C_2H_4 at room temperature for DPPyC3 and nDPPyC3 nanocomposites at 0.5 mm thickness.

Gas	Response time (sec)	
	Sample	
	DPPyC3	nDPPyC3
CO_2	100	100
CH_4	70	100
C_2H_4	60	100

Appendix C Resistance (at response time) to CO_2, CH_4 and C_2H_4 at room temperature for all of the sensor samples

Table C1 Resistance (at response time) to CO_2 at room temperature for all of the sensor samples at various thickness.

Samples	Resistance at response time (ohm)		
	Thickness (mm)		
	0.5	0.8	1.0
PPy	864.4447	868.4182	873.2439
PPyC1	861.4935	862.7536	869.7698
PPyC3	859.3798	859.9213	872.5571
PPyC6	858.0245	858.8286	860.1769
PPyC9	856.5727	856.8342	859.2717
DPPyC3	856.4644	858.1210	860.2910
nDPPyC3	866.0341	-	-

Table C2 Resistance (at response time) to CH_4 at room temperature for all of the sensor samples at various thickness.

Samples	Resistance at response time (ohm)		
	Thickness (mm)		
	0.5	0.8	1.0
PPy	856.1057	857.4935	858.8262
PPyC1	855.9977	856.0584	861.7226
PPyC3	855.9390	856.7513	857.4413
PPyC6	856.2163	857.8184	859.8155
PPyC9	855.9978	856.2273	858.7044
DPPyC3	856.2974	857.1940	862.9388
nDPPyC3	863.8109	-	-

Table C3 Resistance (at response time) to C_2H_4 at room temperature for all of the sensor samples at various thickness.

Samples	Resistance at response time (ohm)		
	Thickness (mm)		
	0.5	0.8	1.0
PPy	868.8566	870.6551	876.9973
PPyC1	866.7790	869.8274	877.4439
PPyC3	866.8763	867.8382	886.6585
PPyC6	866.3393	872.1294	879.2001
PPyC9	861.9167	865.1900	869.2880
DPPyC3	867.6798	869.1928	877.9462
nDPPyC3	862.4135	-	-

Table C4 Resistance (at response time) to CO_2, CH_4 and C_2H_4 at room temperature for DPPyC3 and nDPPyC3 nanocomposite sensors at 0.5 mm thickness.

Gas	Resistance (ohm)	
	Sample	
	DPPyC3	nDPPyC3
CO_2	856.4644	866.0341
CH_4	856.2974	863.8109
C_2H_4	867.6798	862.4135

Appendix D Response time to mixed gases CO_2:CH_4 and CO_2:C_2H_4 at room temperature for all of the sensor samples

Table D1 Response time to CO_2:CH_4 at room temperature for all of the sensor samples at various ratio of gases.

Samples	Response time (sec)		
	Ratio of gas		
	1:1	1:2	1:3
PPy	60	60	80
PPyC1	60	60	70
PPyC3	60	60	40
PPyC6	60	70	50
PPyC9	60	70	60
DPPyC3	50	70	40
nDPPyC3	60	70	70

Table D2 Response time to CO_2:C_2H_4 at room temperature for all of the sensor samples at various ratio of gases.

Samples	Response time (sec)		
	Ratio of gas		
	1:1	1:2	1:3
PPy	70	90	60
PPyC1	100	90	90
PPyC3	60	90	90
PPyC6	90	80	90
PPyC9	80	80	60
DPPyC3	80	70	60
nDPPyC3	90	80	80

Appendix E Resistance (at response time) to the mixed gases CO_2:CH_4 and CO_2:C_2H_4 at room temperature for all of the sensor samples

Table E1 Resistance (at response time) to CO_2:CH_4 at room temperature for all of the sensor samples at various ratio of gases.

Samples	Resistance (ohm)		
	Ratio of gas		
	1:1	1:2	1:3
PPy	857.7367	871.8548	877.2915
PPyC1	860.7707	872.6221	874.8788
PPyC3	863.3079	871.8249	876.7907
PPyC6	865.9308	872.4253	876.9215
PPyC9	865.3329	874.3874	876.6980
DPPyC3	868.0375	870.8457	877.0383
nDPPyC3	867.6148	874.9236	875.9078

Table E2 Resistance (at response time) to CO_2:C_2H_4 at room temperature for all of the sensor samples at various ratio of gases.

Samples	Resistance (ohm)		
	Ratio of gas		
	1:1	1:2	1:3
PPy	856.1750	873.0986	875.2983
PPyC1	858.3315	872.9095	873.5396
PPyC3	864.5911	874.0054	876.0309
PPyC6	866.6203	874.1402	876.8197
PPyC9	870.5780	872.0120	876.3817
DPPyC3	873.1713	878.4388	871.9793
nDPPyC3	872.0343	877.6899	871.2575

Appendix F Calculation of Cross sensitivity (%) at room temperature for all of the samples sensor to CO_2:CH_4 and CO_2:C_2H_4

Table F1 Resistance to CO_2 (0.1 bar) and the mixture of CO_2 and CH_4 at room temperature for all of the sensor samples.

Sample	Resistance (ohm)			
	R_{CO2}	$R_{CO2:CH4}$	$R_{CO2:2CH4}$	$R_{CO2:3CH4}$
PPy	864.4447	857.7367	871.8548	877.2915
PPyC1	861.4935	860.7707	872.6221	874.8788
PPyC3	859.3798	863.3079	871.8249	876.7907
PPyC6	858.0245	865.9308	872.4235	876.9215
PPyC9	856.5727	865.3329	874.3874	876.6980
DPPyC3	856.4644	868.0375	870.8457	877.0383
nDPPyC3	866.0341	867.6148	874.9236	875.9078

Table F2 Resistance to CH_4 at room temperature for all of the sensor samples at various gas pressures.

Samples	Resistance at response time (ohm)		
	Pressure (bars)		
	0.1	0.2	0.3
PPy	856.1057	857.4935	858.8262
PPyC1	855.9977	857.0584	858.7226
PPyC3	855.9390	856.7513	857.4413
PPyC6	856.2163	857.8184	859.8155
PPyC9	855.9978	856.2273	857.2044
DPPyC3	856.2974	857.1940	858.9388
nDPPyC3	863.8109	864.3329	865.7936

Calculation for Cross sensitivity (%)

CO_2:CH_4 (1:1)

PPy

$R_{CO2+CH4}$	=	857.7367	ohm
R_{CO2}	=	864.4447	ohm
R_{CH4}	=	856.1057	ohm
Cross sensitivity to CO_2	=	857.7367/864.4447	
	=	0.9922	
	=	99.22 %	
Cross sensitivity to CH_4	=	857.7367/856.1057	
	=	1.0019	
	=	100.19 %	

Similar calculation was used for all the samples and for all the ratios of gas mixtures.

Table F3 Resistance to CO_2 (0.1 bar) and the mixture of CO_2 and C_2H_4 at room temperature for all of the sensor samples.

Sample	Resistance (ohm)			
	R_{CO2}	$R_{CO2:C2H4}$	$R_{CO2:2C2H4}$	$R_{CO2:3C2H4}$
PPy	864.4447	856.1750	873.0986	875.2983
PPyC1	861.4935	858.3315	872.9095	873.5396
PPyC3	859.3798	864.5911	874.0054	876.0309
PPyC6	858.0245	866.6203	874.1402	876.8197
PPyC9	856.5727	870.5780	872.0120	876.3817
DPPyC3	856.4644	873.1713	878.4388	871.9793
nDPPyC3	866.0341	872.0343	877.6899	871.2575

Table F4 Resistance to C_2H_4 at room temperature for all of the sensor samples at various gas pressures.

Samples	Resistance at response time (ohm)		
	Pressure (bars)		
	0.1	0.2	0.3
PPy	868.8566	870.6551	872.9973
PPyC1	866.7790	869.8274	872.4439
PPyC3	866.8763	867.8382	869.6585
PPyC6	866.3393	870.1294	874.2001
PPyC9	861.9167	865.1900	869.2880
DPPyC3	867.6798	869.0700	871.9462
nDPPyC3	862.4135	864.0021	865.9852

Calculation for Cross sensitivity (%)

CO_2:C_2H_4 (1:1)

PPy

$R_{CO2+C2H4}$ = 856.1750 ohm

R_{CO2} = 864.4447 ohm

R_{C2H4} = 868.8566 ohm

Cross sensitivity to CO_2 = 856.1750/864.4447

= 0.9904

= 99.04 %

Cross sensitivity to C_2H_4 = 856.1750/868.8566

= 0.9854

= 98.54 %

Similar calculation was used for all the samples and for all the ratios of gas mixtures.

Appendix G Raw data of resistance vs. time obtained from the electrometer

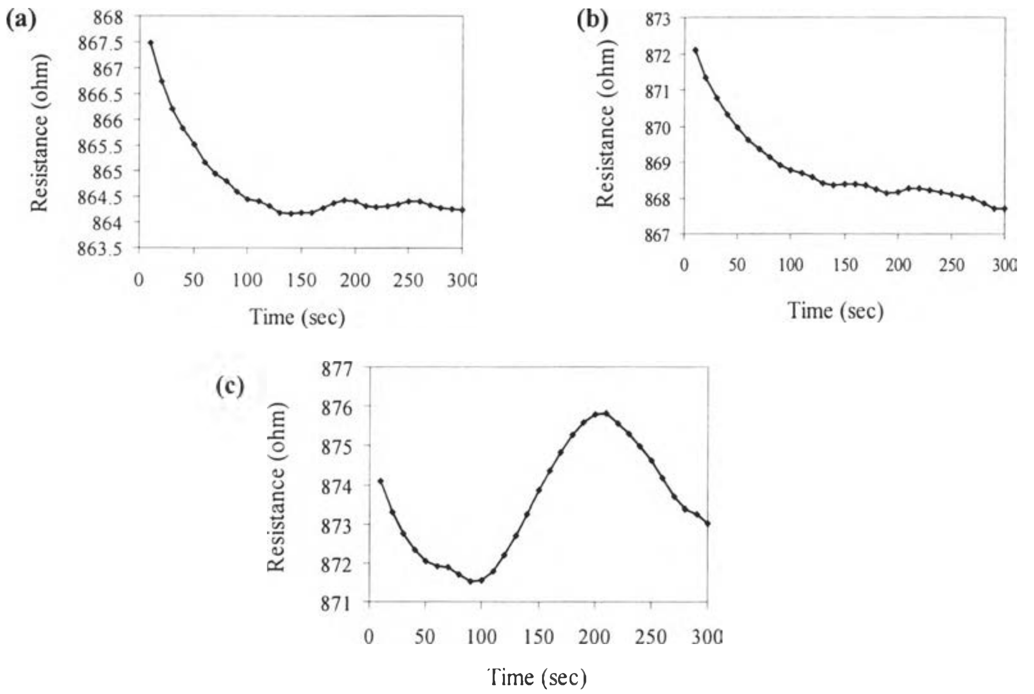

Figure G1 Resistance vs. time under CO_2 for PPy of (a) 0.5, (b) 0.8 and (c) 1.0mm thick.

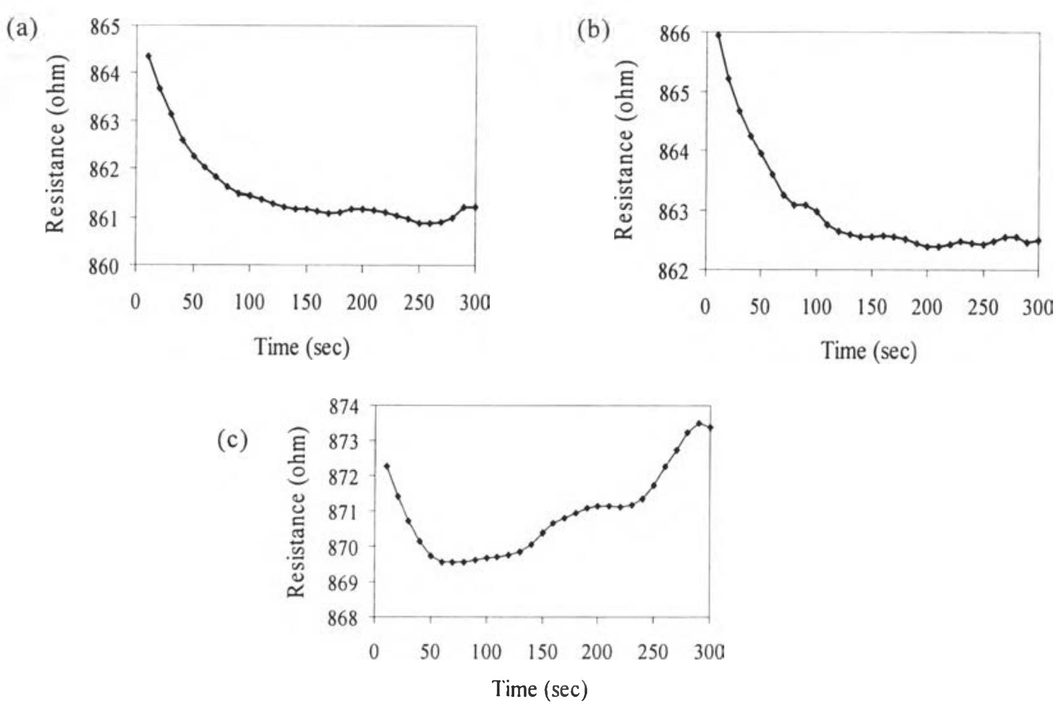

Figure G2 Resistance vs. time under CO_2 for PPyC1 of (a) 0.5, (b) 0.8 and (c) 1.0mm thick.

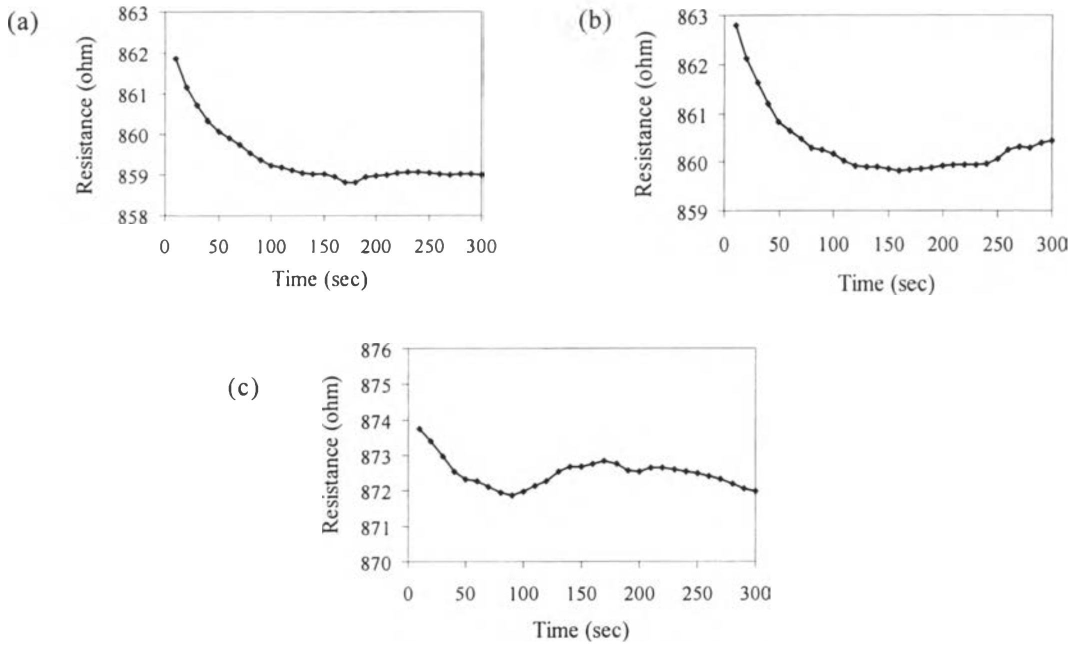

Figure G3 Resistance vs. time under CO_2 for PPyC3 of (a) 0.5, (b) 0.8 and (c) 1.0mm thick.

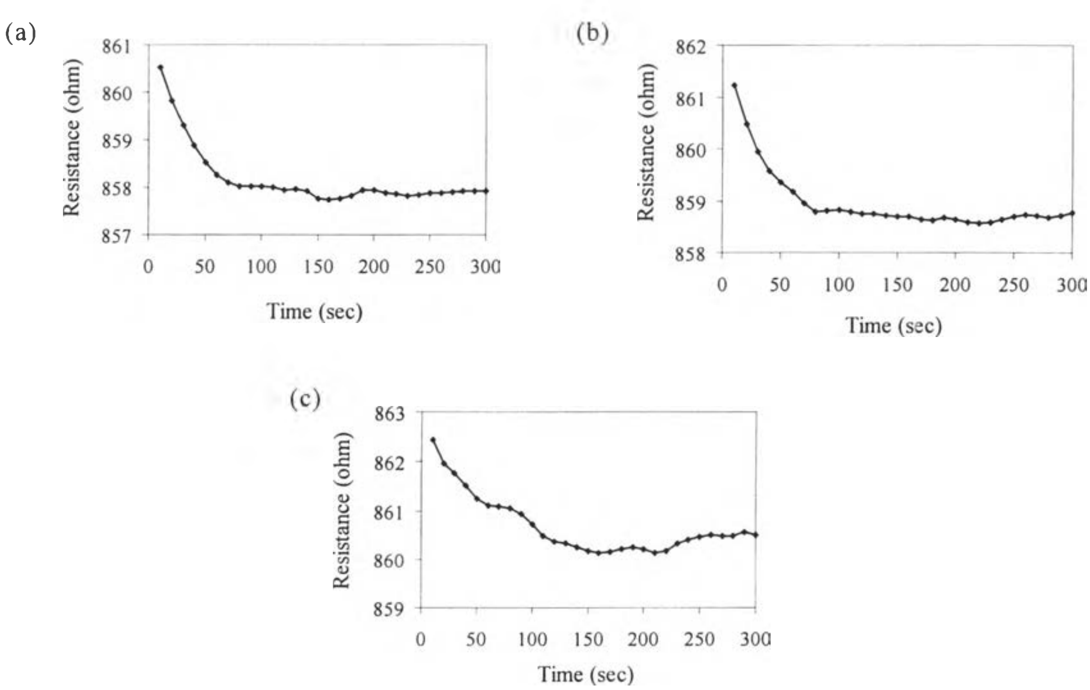

Figure G4 Resistance vs. time under CO_2 for PPyC6 of (a) 0.5, (b) 0.8 and (c) 1.0mm thick.

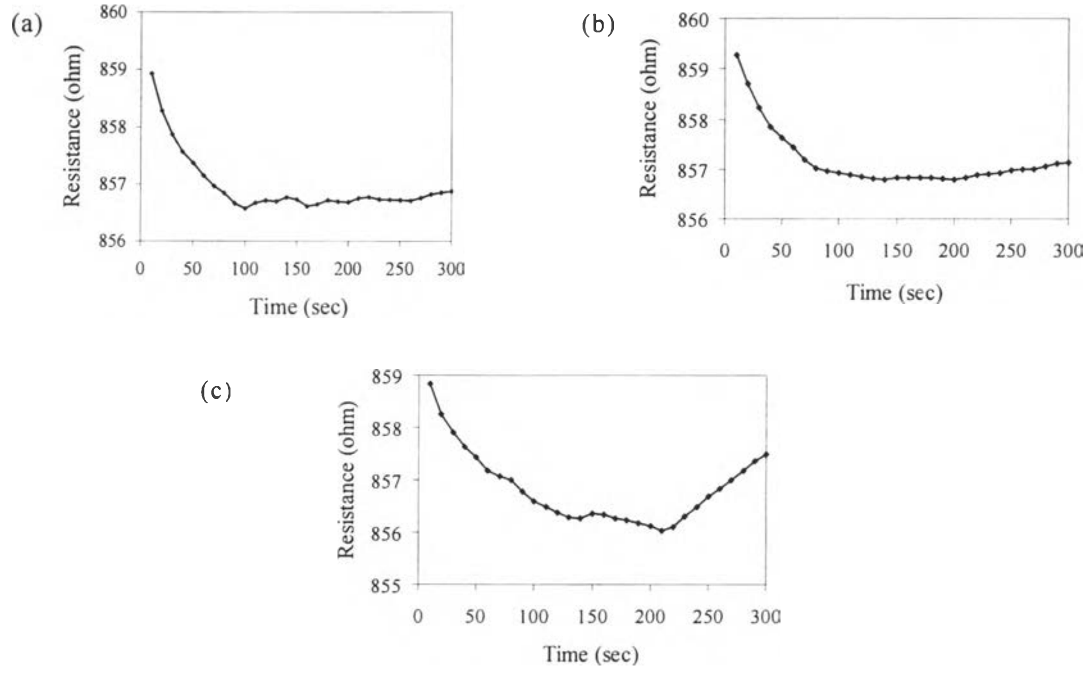

Figure G5 Resistance vs. time under CO_2 for PPyC9 of (a) 0.5, (b) 0.8 and (c) 1.0mm thick.

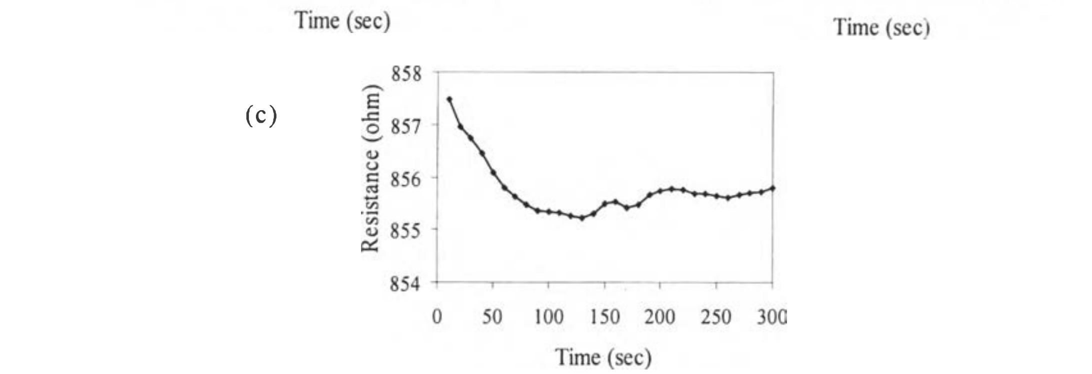

Figure G6 Resistance vs. time under CO_2 for DPPyC3 of (a) 0.5, (b) 0.8 and (c) 1.0mm thick.

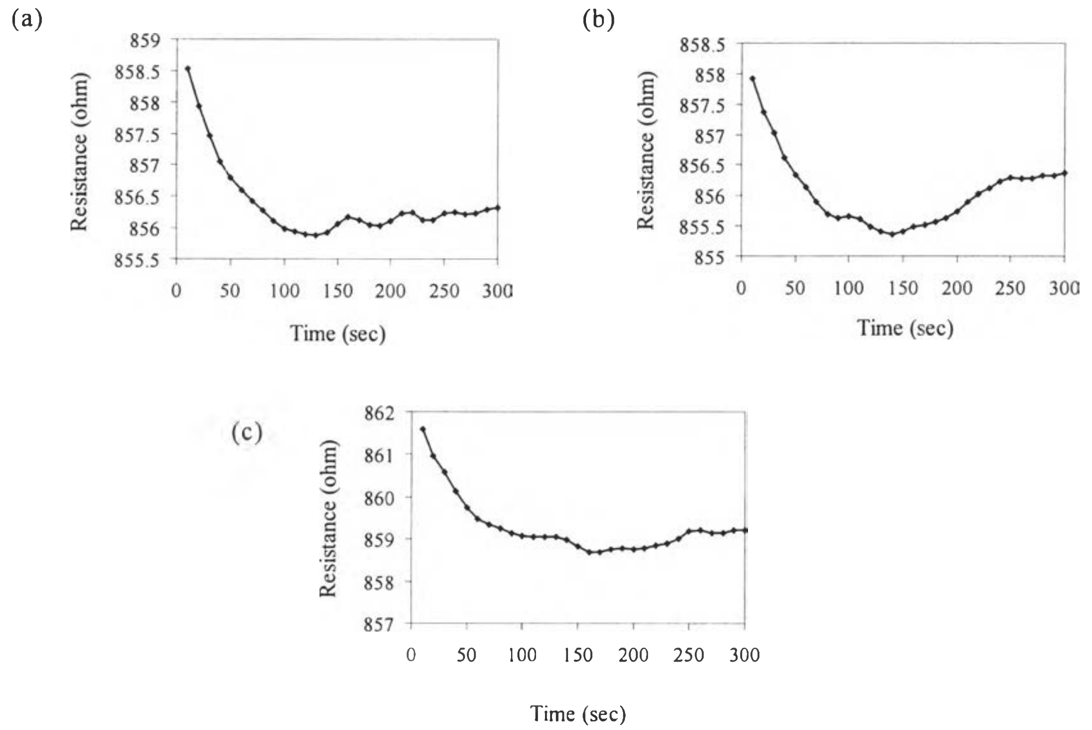

Figure G7 Resistance vs. time under CH_4 for PPy of (a) 0.5, (b) 0.8 and (c) 1.0mm thick.

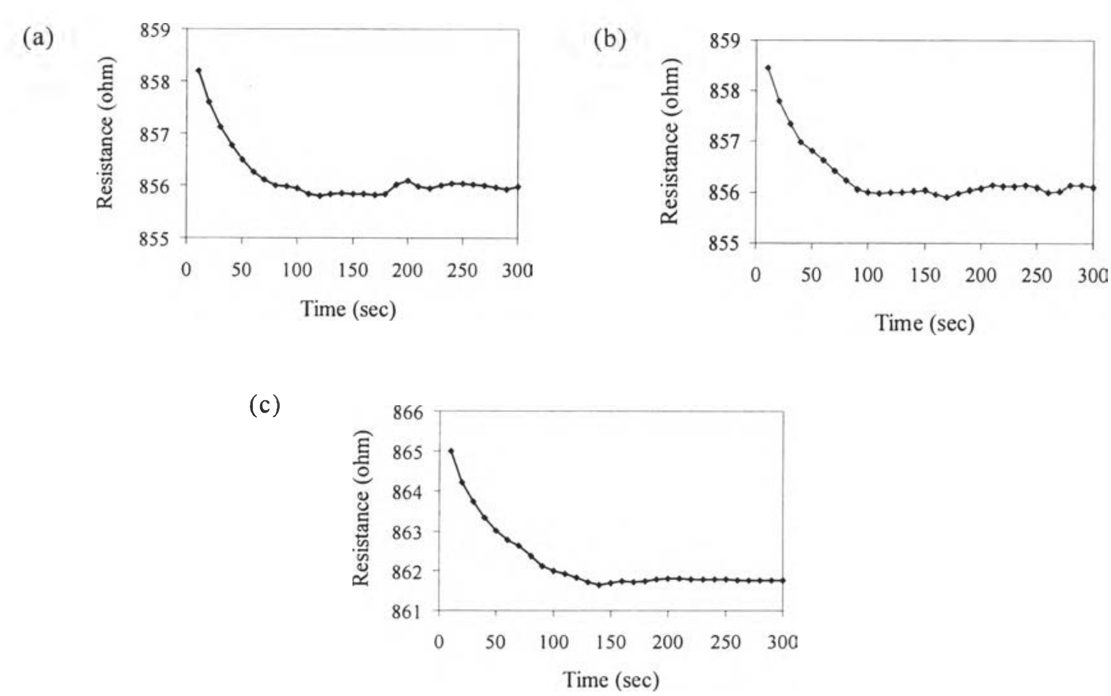

Figure G8 Resistance vs. time under CH_4 for PPyCl of (a) 0.5, (b) 0.8 and (c) 1.0mm thick.

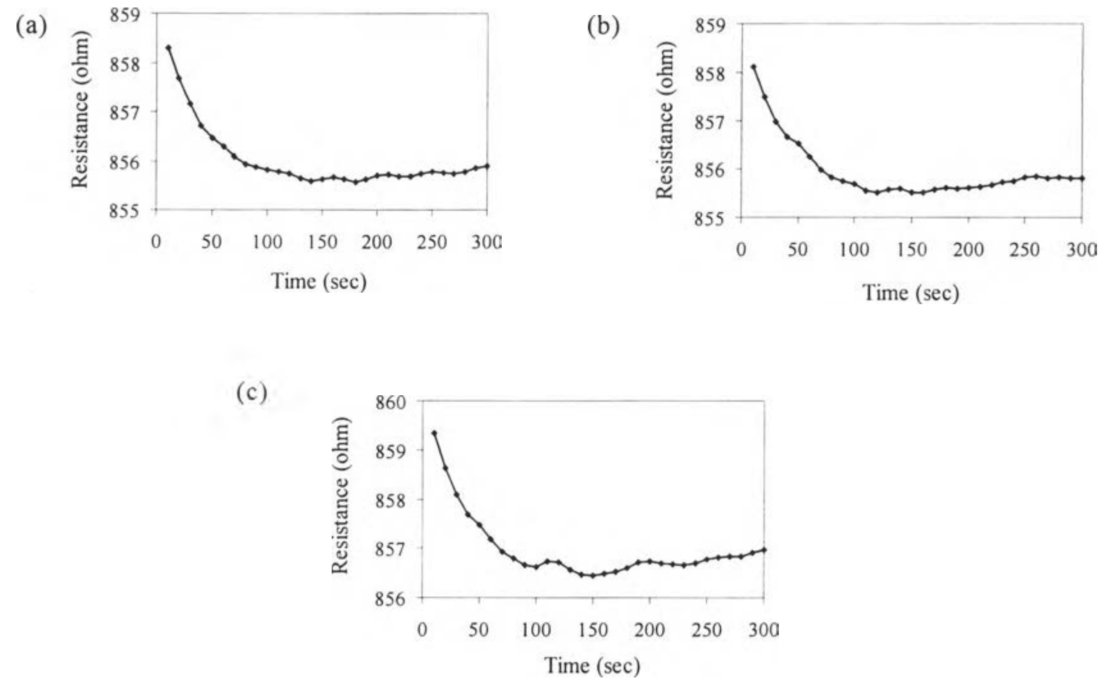

Figure G9 Resistance vs. time under CH_4 for PPyC3 of (a) 0.5, (b) 0.8 and (c) 1.0mm thick.

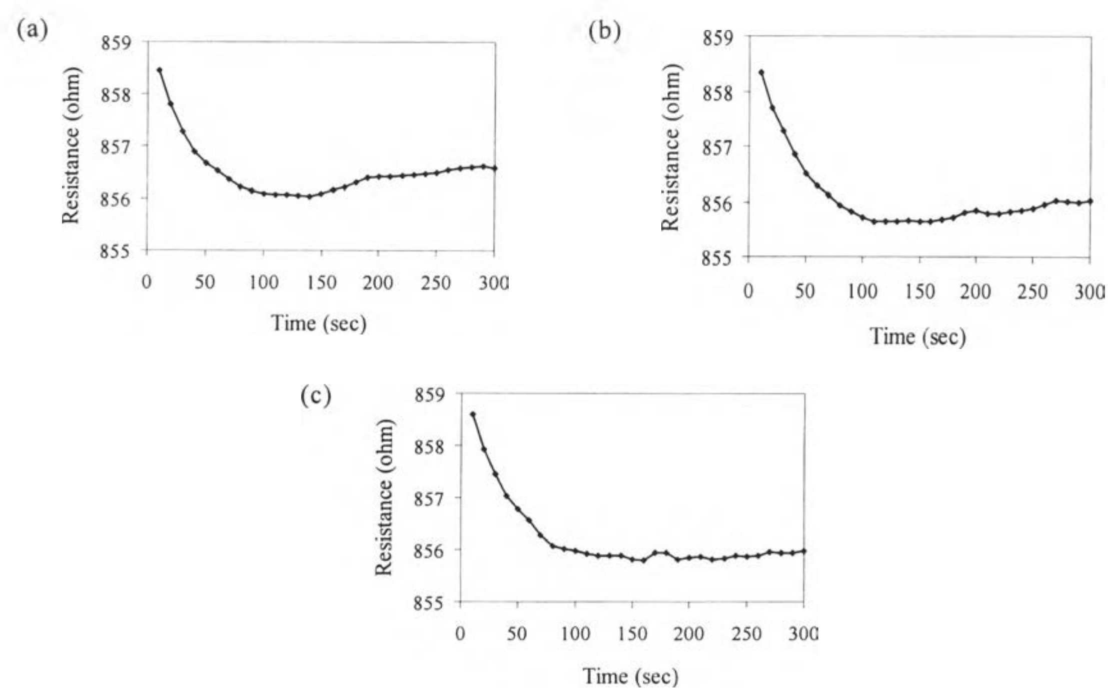

Figure G10 Resistance vs. time under CH_4 for PPyC6 of (a) 0.5, (b) 0.8 and (c) 1.0mm thick.

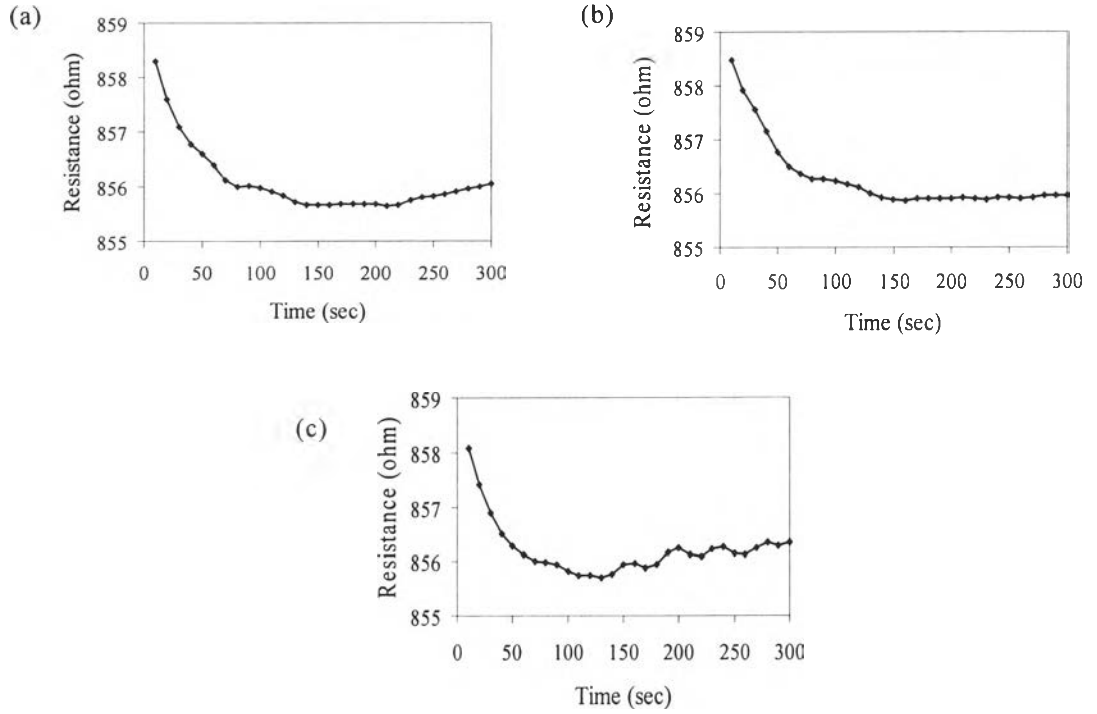

Figure G11 Resistance vs. time under CH_4 for PPyC9 of (a) 0.5, (b) 0.8 and (c) 1.0mm thick.

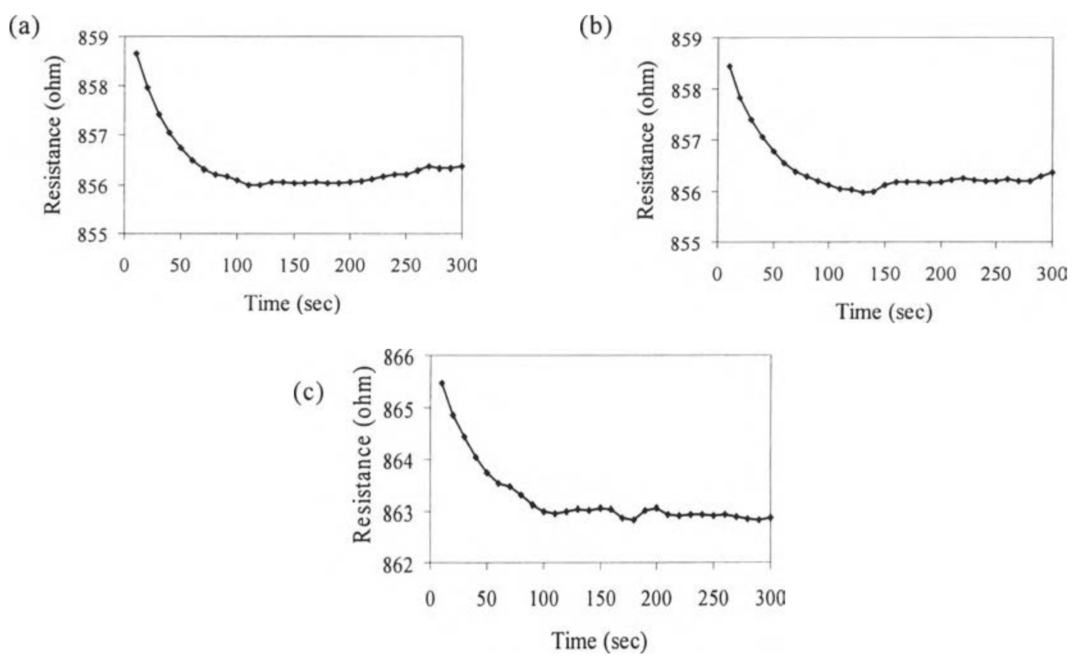

Figure G12 Resistance vs. time under CH_4 for DPPyC3 of (a) 0.5, (b) 0.8 and (c) 1.0mm thick.

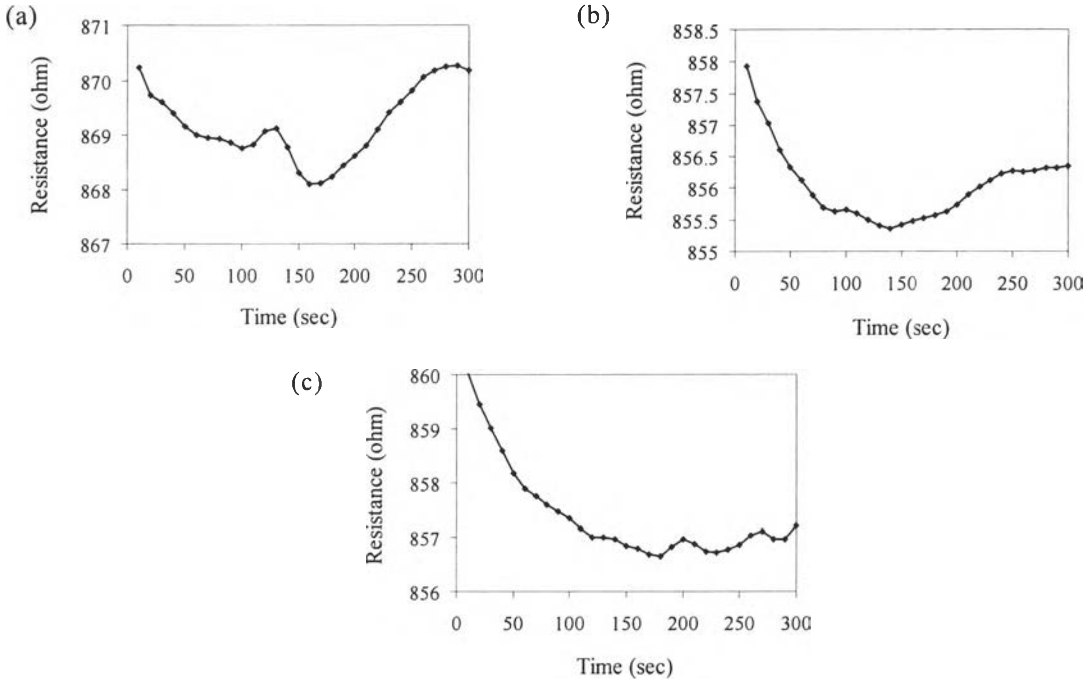

Figure G13 Resistance vs. time under C_2H_4 for PPy of (a) 0.5, (b) 0.8 and (c) 1.0mm thick.

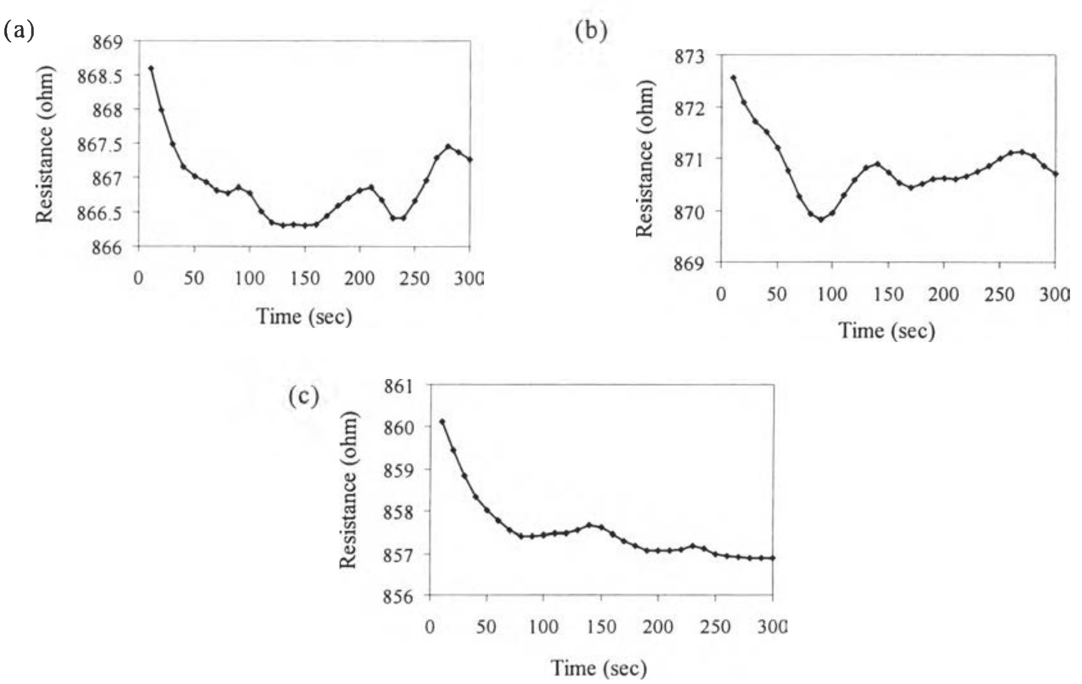

Figure G14 Resistance vs. time under C_2H_4 for PPyCl of (a) 0.5, (b) 0.8 and (c) 1.0mm thick.

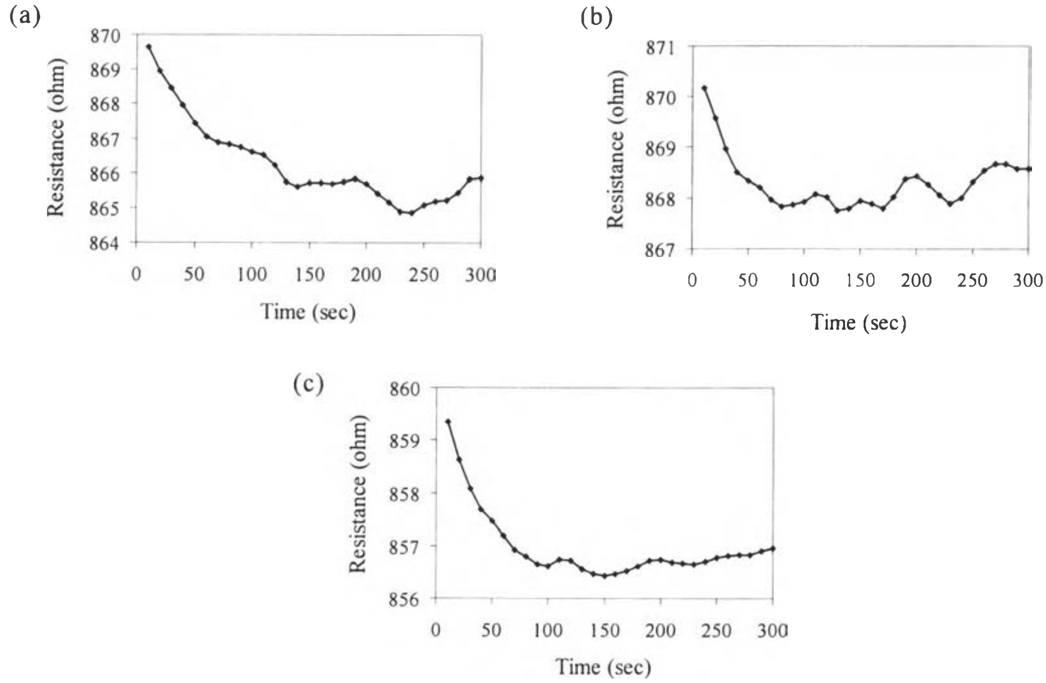

Figure G15 Resistance vs. time under C_2H_4 for PPyC3 of (a) 0.5, (b) 0.8 and (c) 1.0mm thick.

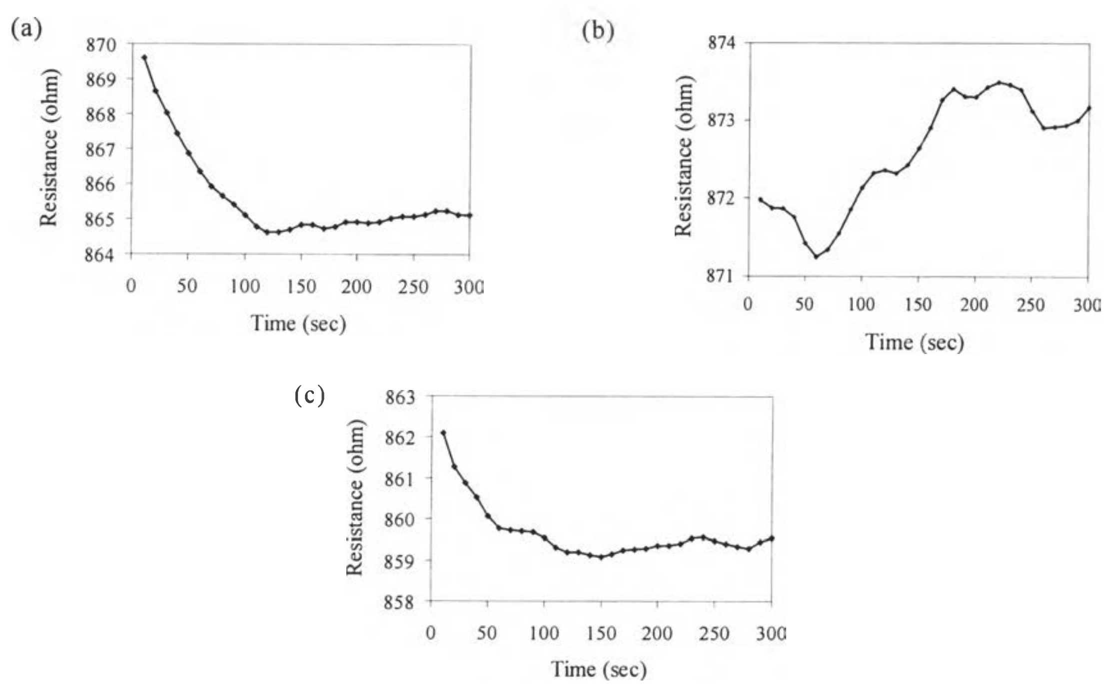

Figure G16 Resistance vs. time under C_2H_4 for PPyC6 of (a) 0.5, (b) 0.8 and (c) 1.0mm thick.

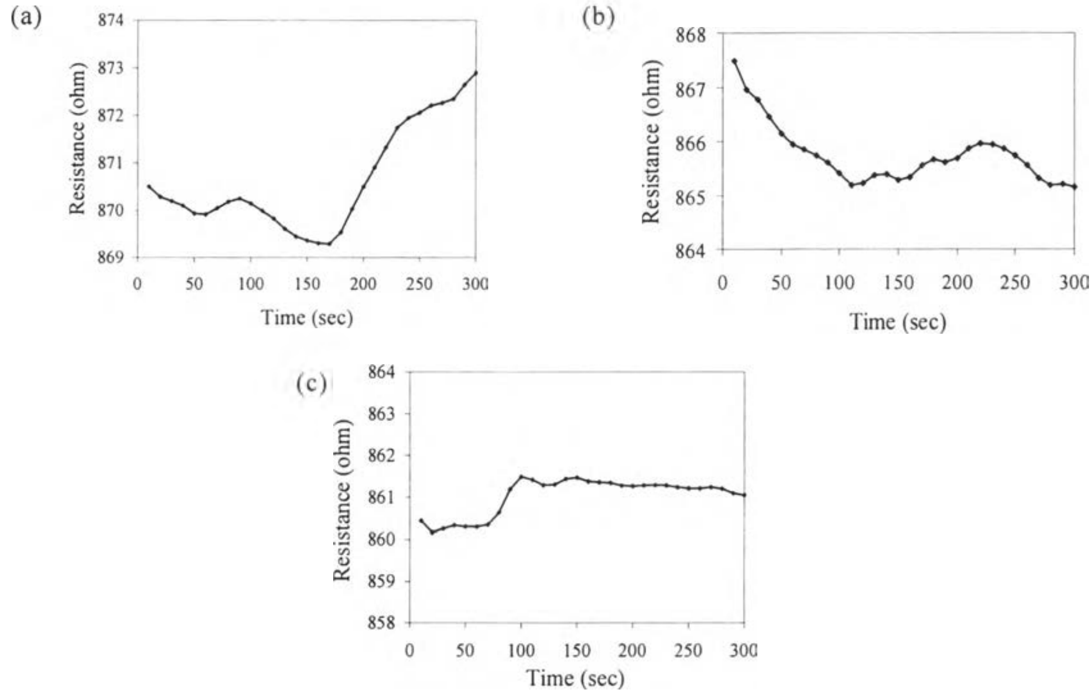

Figure G17 Resistance vs. time under C_2H_4 for PPyC9 of (a) 0.5, (b) 0.8 and (c) 1.0mm thick.

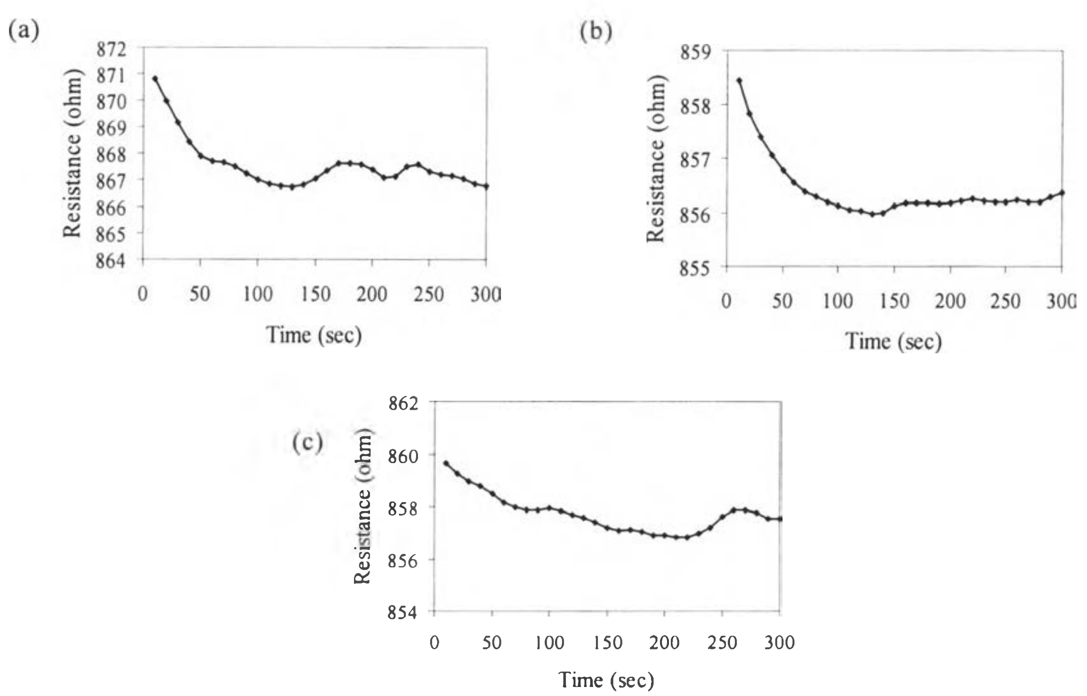

Figure G18 Resistance vs. time under C_2H_4 for DPPyC3 of (a) 0.5, (b) 0.8 and (c) 1.0mm thick.

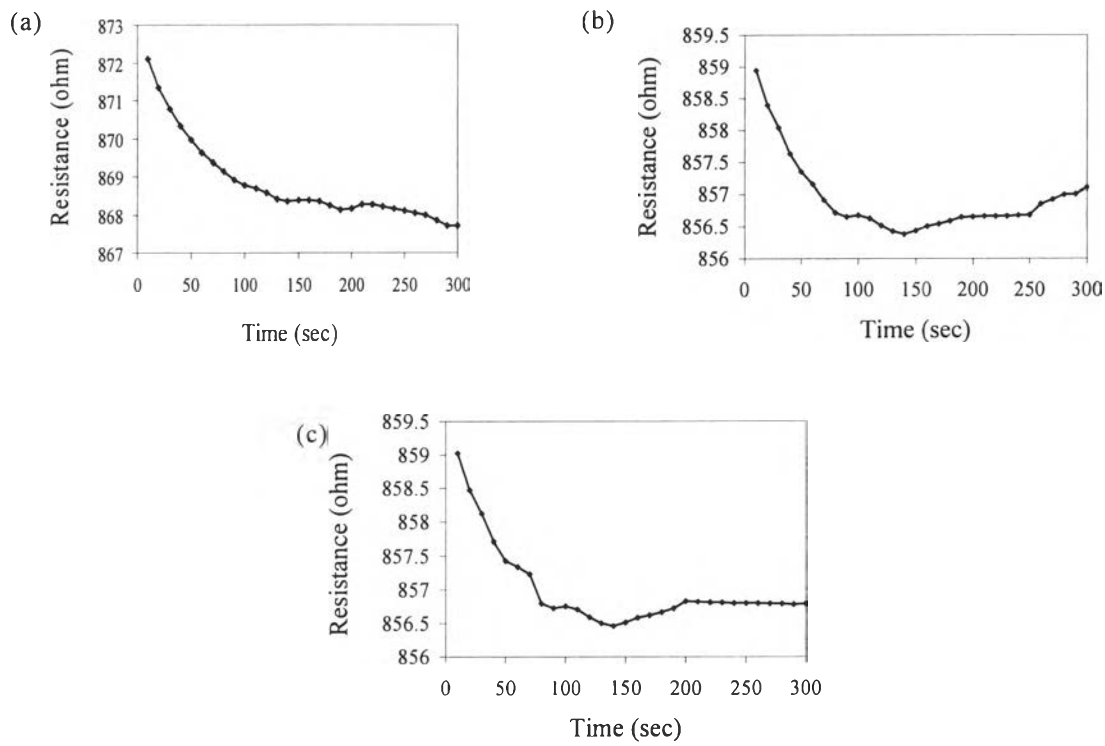

Figure G19 Resistance vs. time for PPy under (a) CO_2, (b) CH_4 and (c) C_2H_4 at the gas pressure of 0.2 bars.

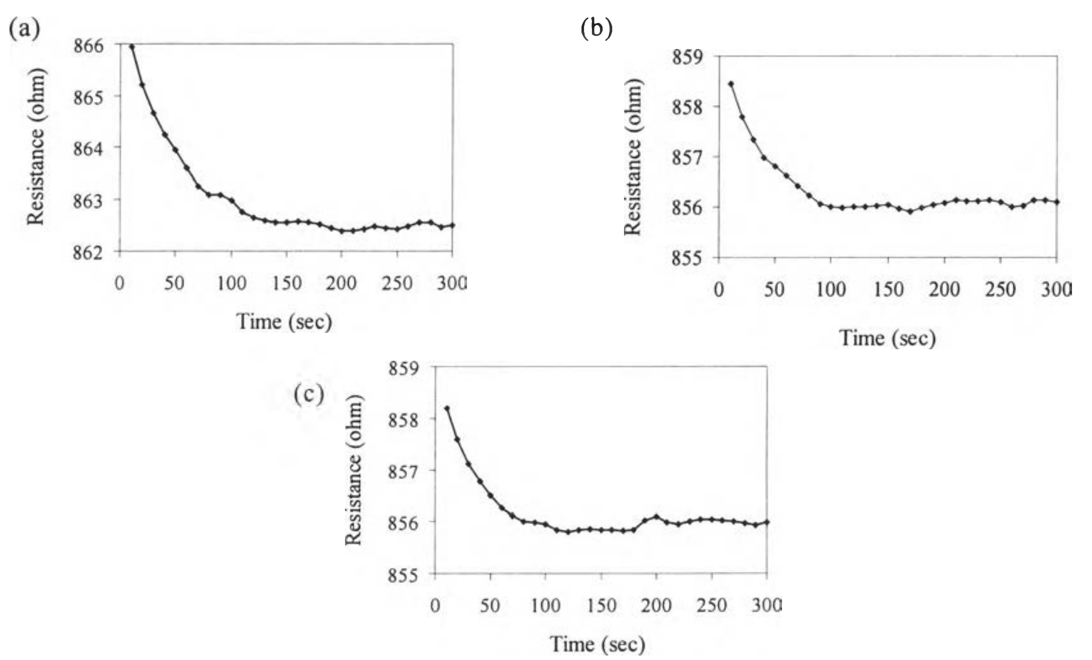

Figure G20 Resistance vs. time for PPyCl under (a) CO_2, (b) CH_4 and (c) C_2H_4 at the gas pressure of 0.2 bars.

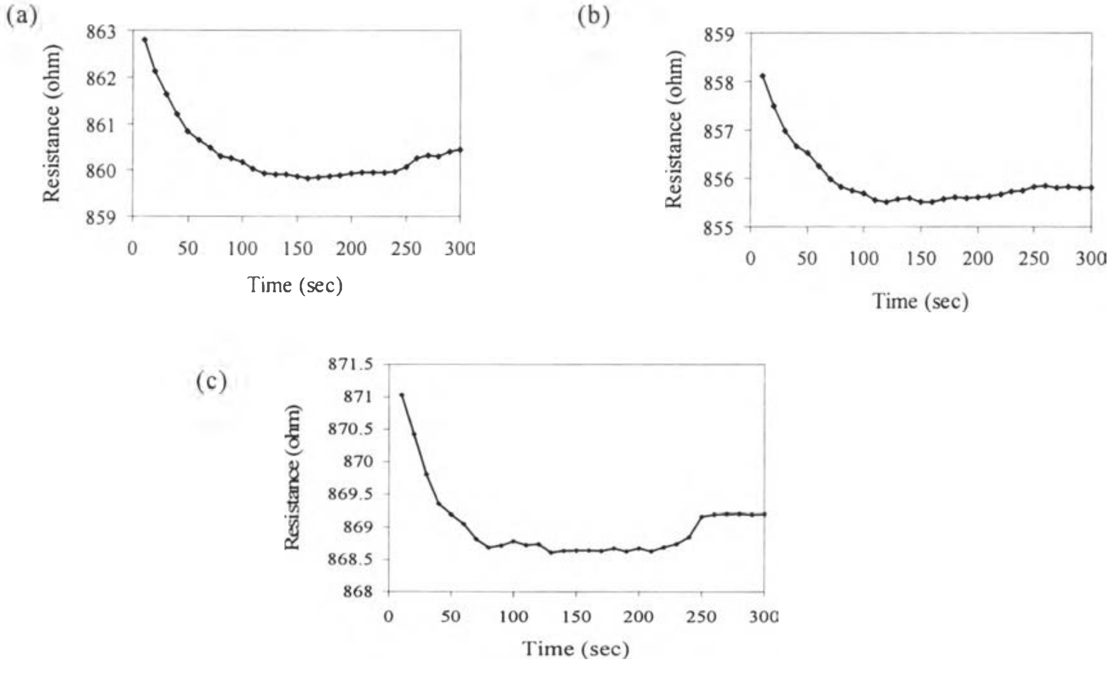

Figure G21 Resistance vs. time for PPyC3 under (a) CO_2, (b) CH_4 and (c) C_2H_4 at the gas pressure of 0.2 bars.

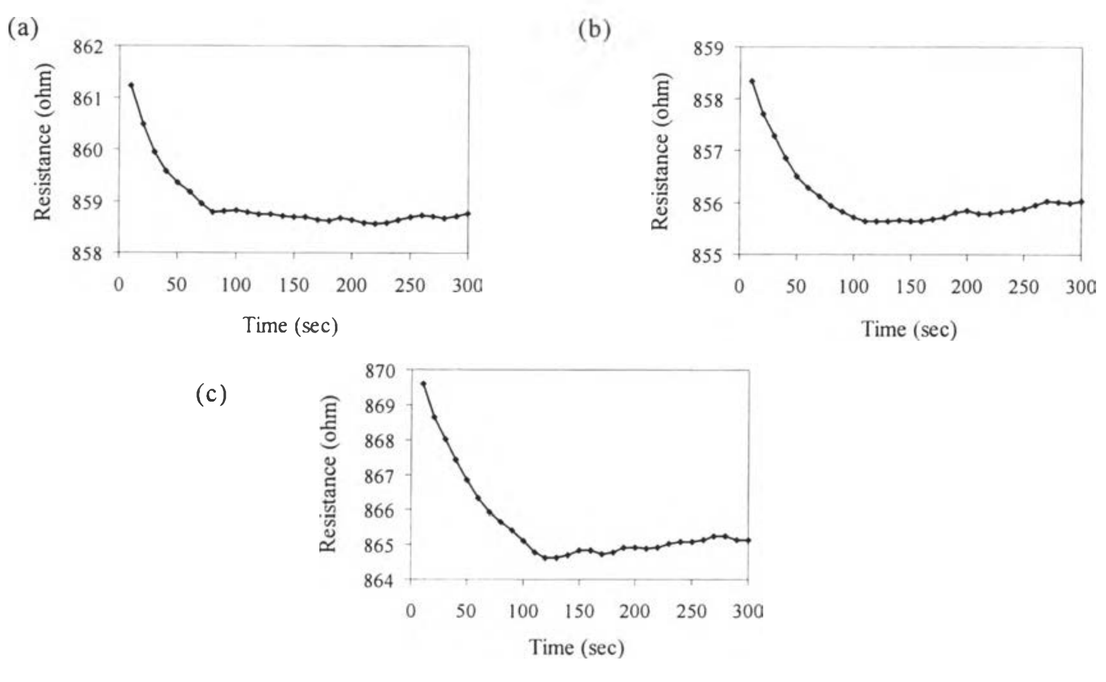

Figure G22 Resistance vs. time for PPyC6 under (a) CO_2, (b) CH_4 and (c) C_2H_4 at the gas pressure of 0.2 bars.

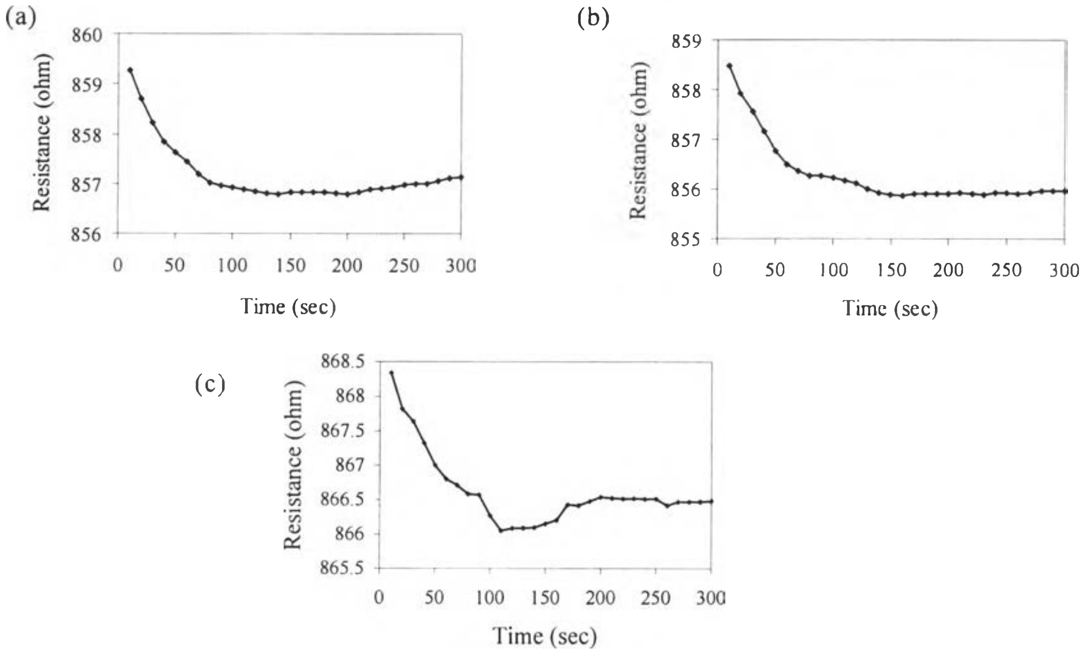

Figure G23 Resistance vs. time for PPyC9 under (a) CO_2, (b) CH_4 and (c) C_2H_4 at the gas pressure of 0.2 bars.

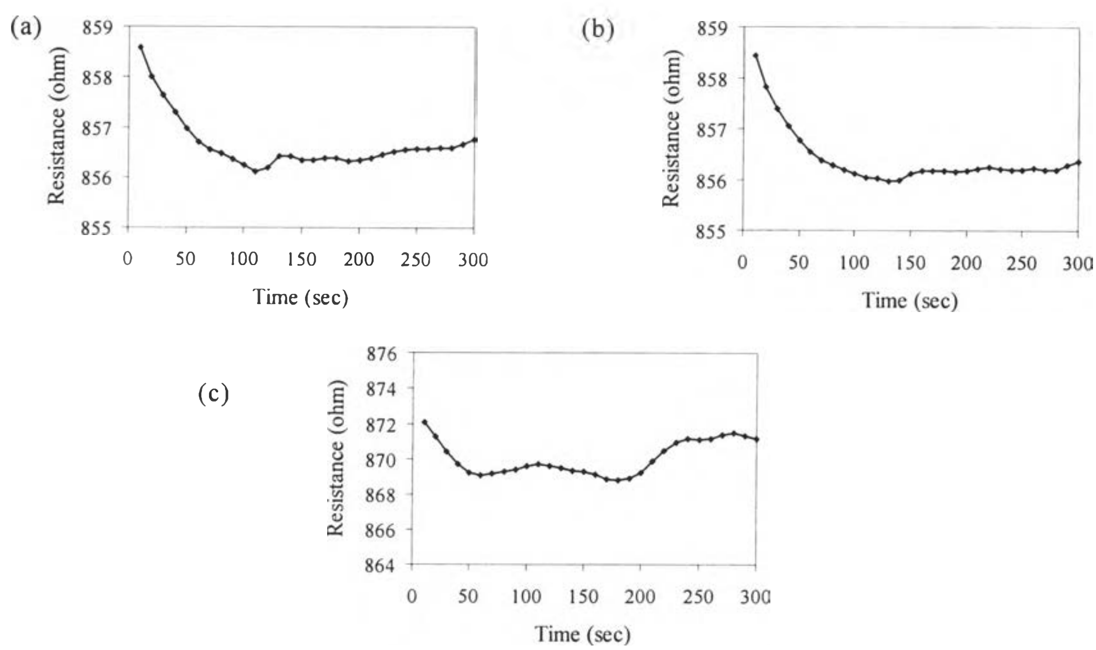

Figure G24 Resistance vs. time for DPPyC3 under (a) CO_2, (b) CH_4 and (c) C_2H_4 at the gas pressure of 0.2 bars.

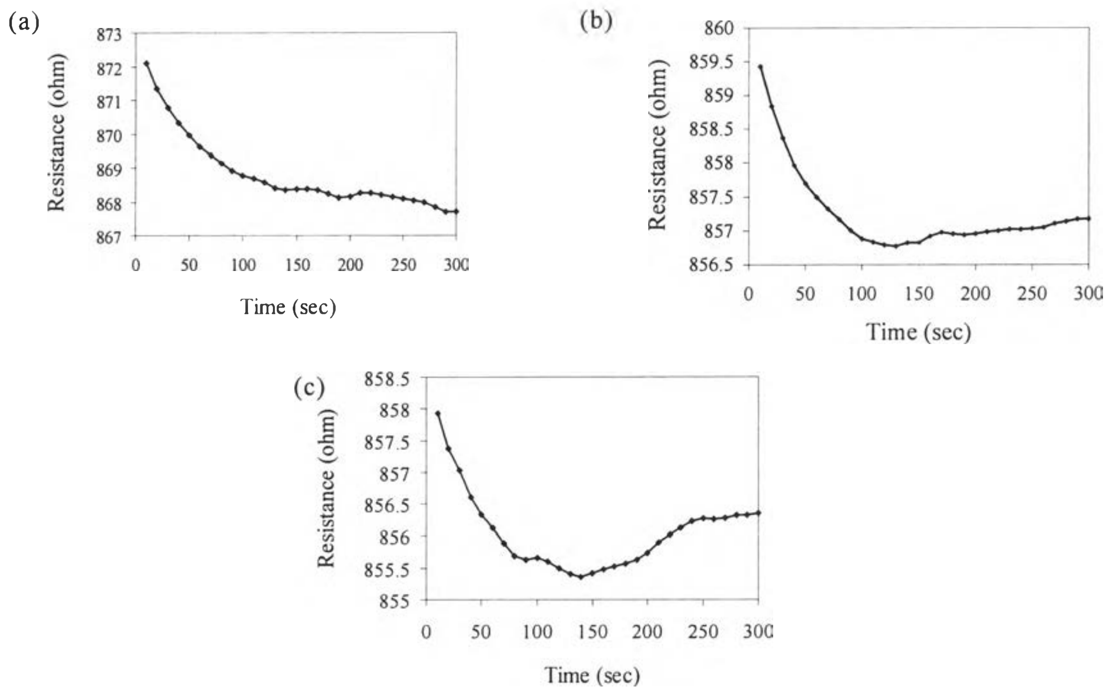

Figure G25 Resistance vs. time for nDPPyC3 under (a) CO_2, (b) CH_4 and (c) C_2H_4 at the gas pressure of 0.2 bars.

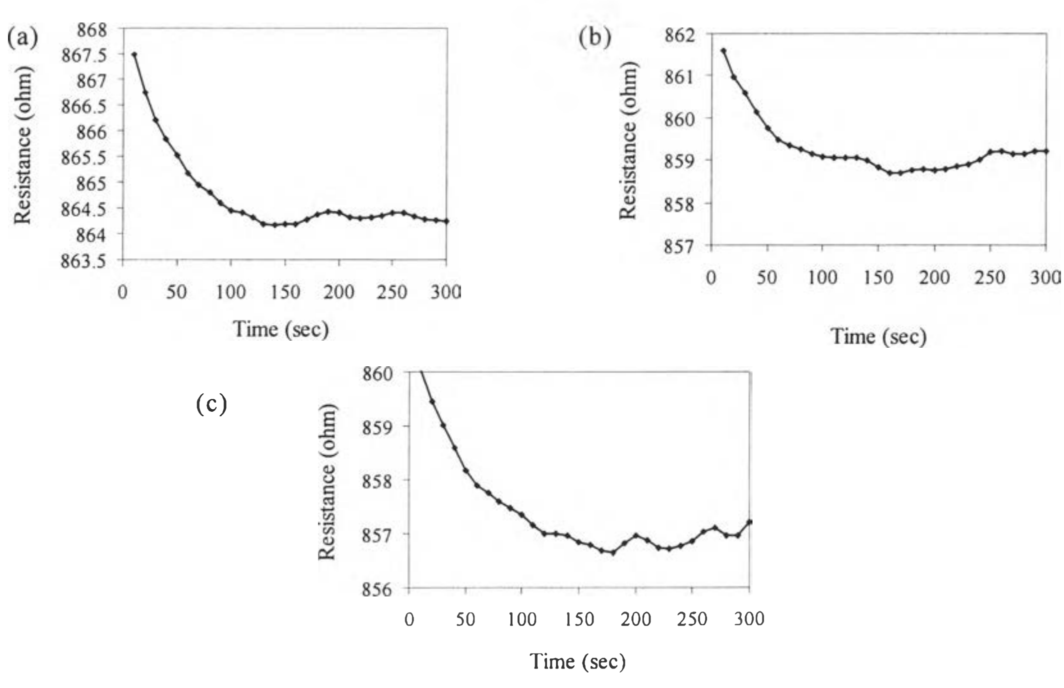

Figure G26 Resistance vs. time for PPy under (a) CO_2, (b) CH_4 and (c) C_2H_4 at the gas pressure of 0.3 bars.

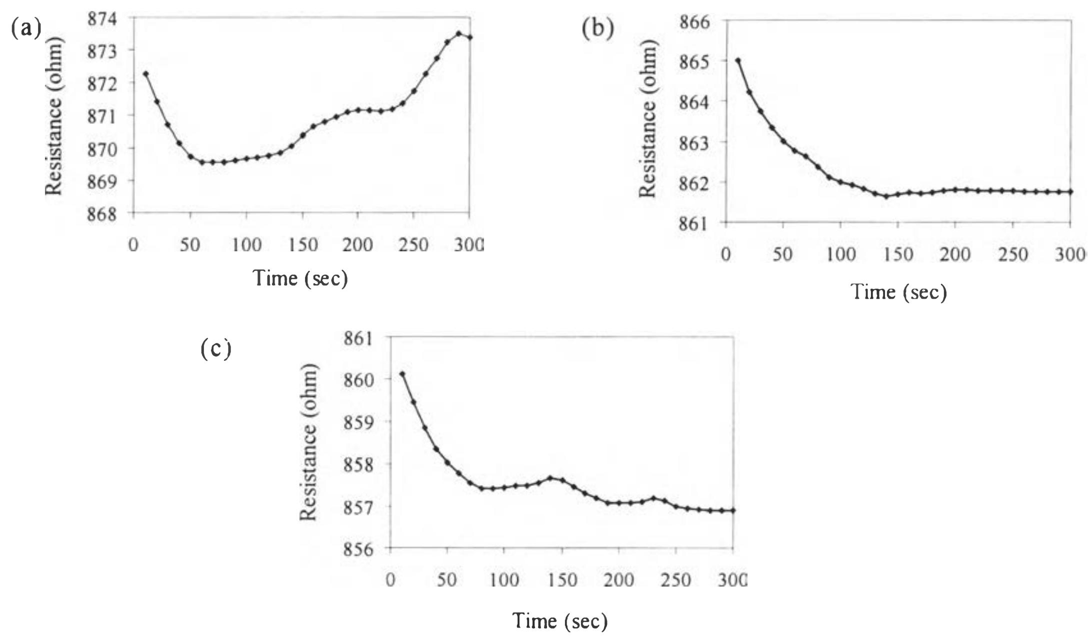

Figure G27 Resistance vs. time for PPyC1 under (a) CO_2, (b) CH_4 and (c) C_2H_4 at the gas pressure of 0.3 bars.

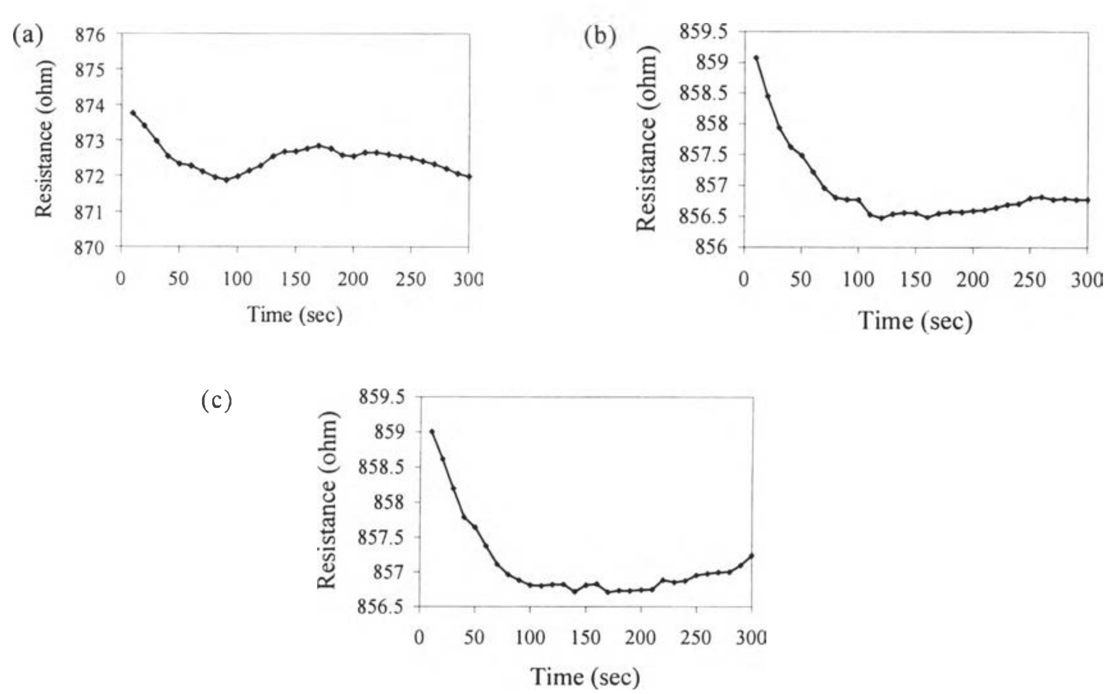

Figure G28 Resistance vs. time for PPyC3 under (a) CO_2, (b) CH_4 and (c) C_2H_4 at the gas pressure of 0.3 bars.

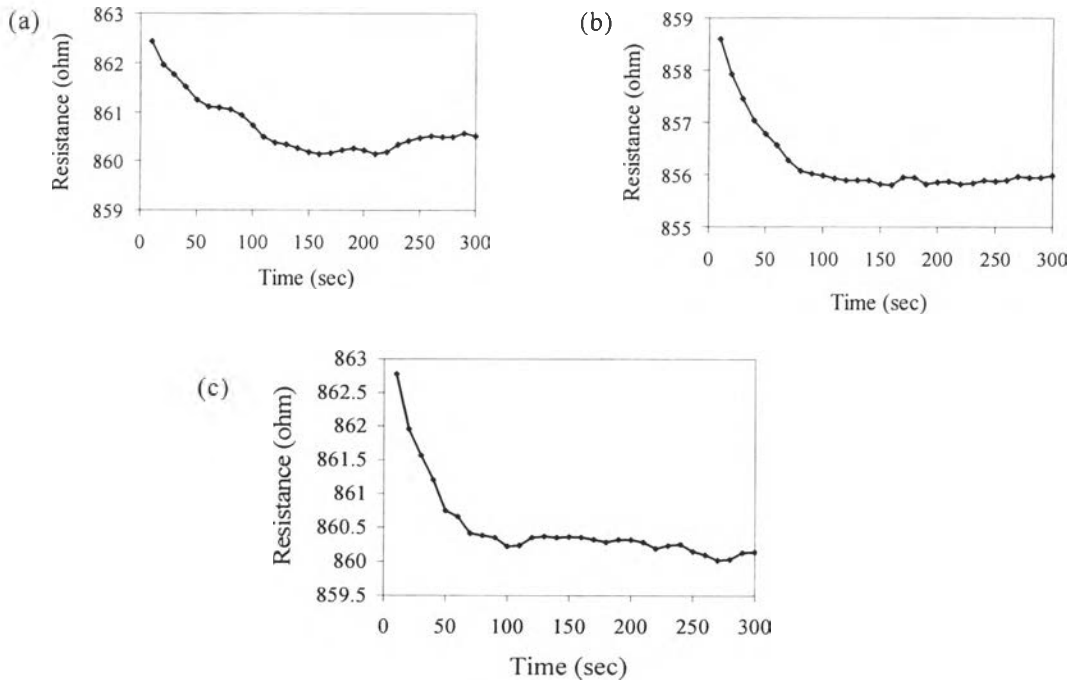

Figure G29 Resistance vs. time for PPyC6 under (a) CO_2, (b) CH_4 and (c) C_2H_4 at the gas pressure of 0.3 bars.

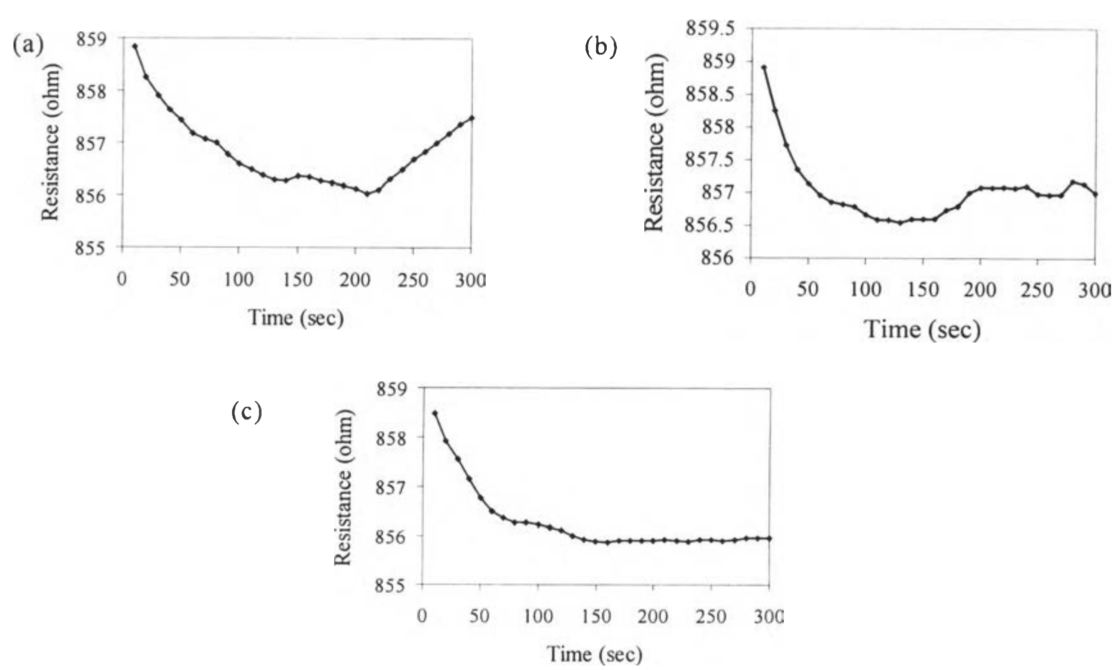

Figure G30 Resistance vs. time for PPyC9 under (a) CO_2, (b) CH_4 and (c) C_2H_4 at the gas pressure of 0.3 bars.

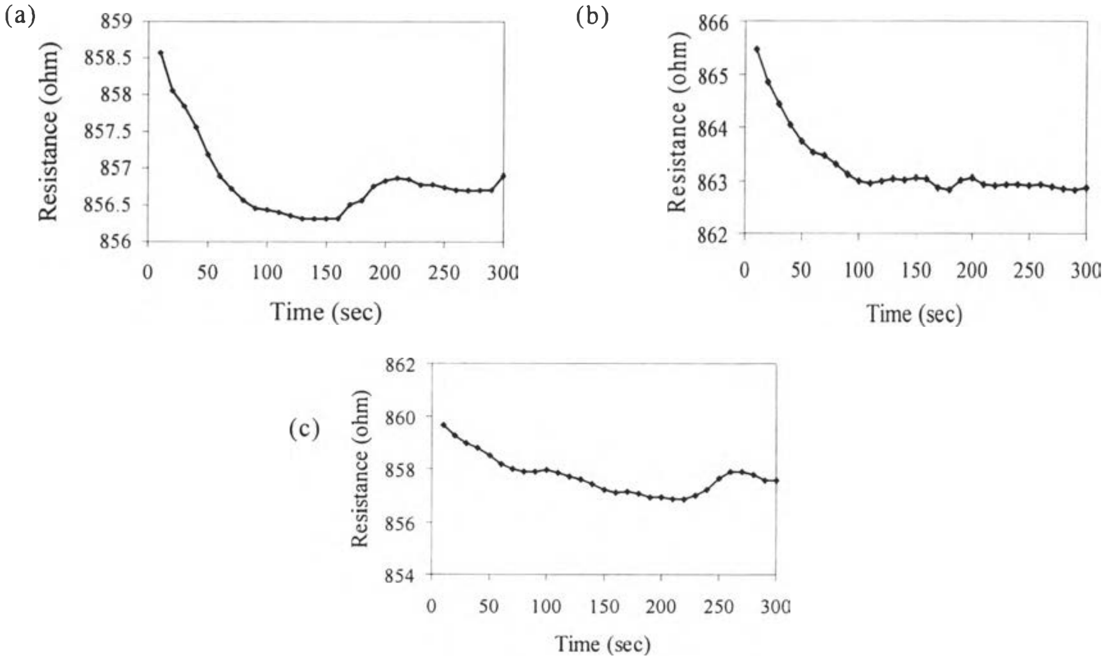

Figure G31 Resistance vs. time for DPPyC3 under (a) CO_2, (b) CH_4 and (c) C_2H_4 at the gas pressure of 0.3 bars.

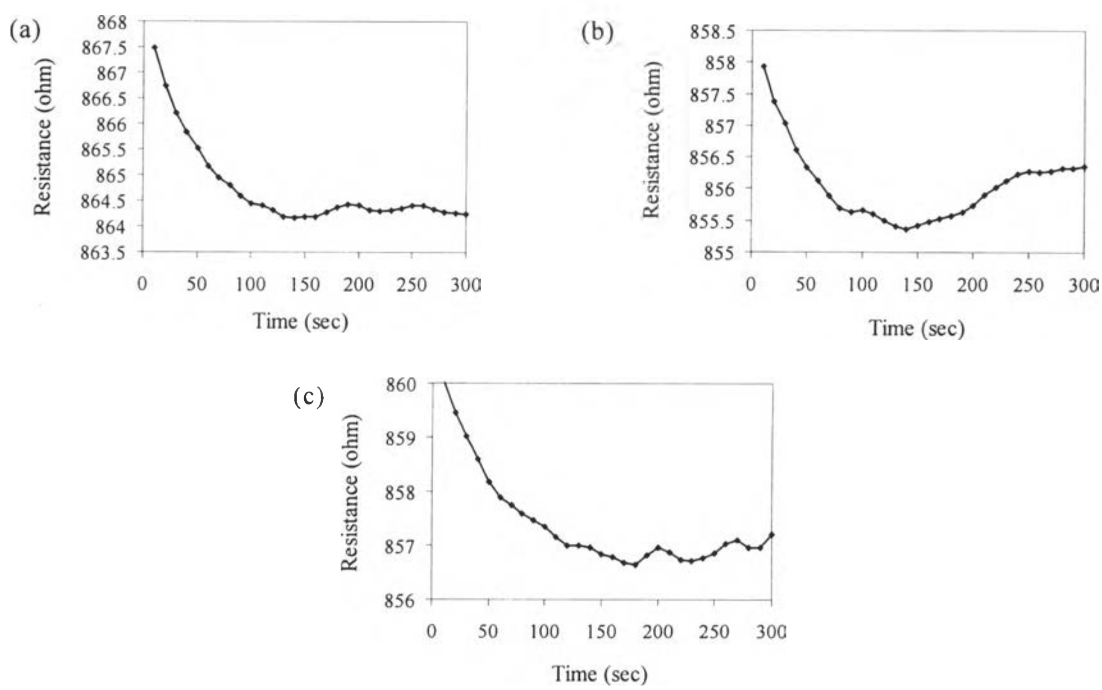

Figure G32 Resistance vs. time for nDPPyC3 under (a) CO_2, (b) CH_4 and (c) C_2H_4 at the gas pressure of 0.3 bars.

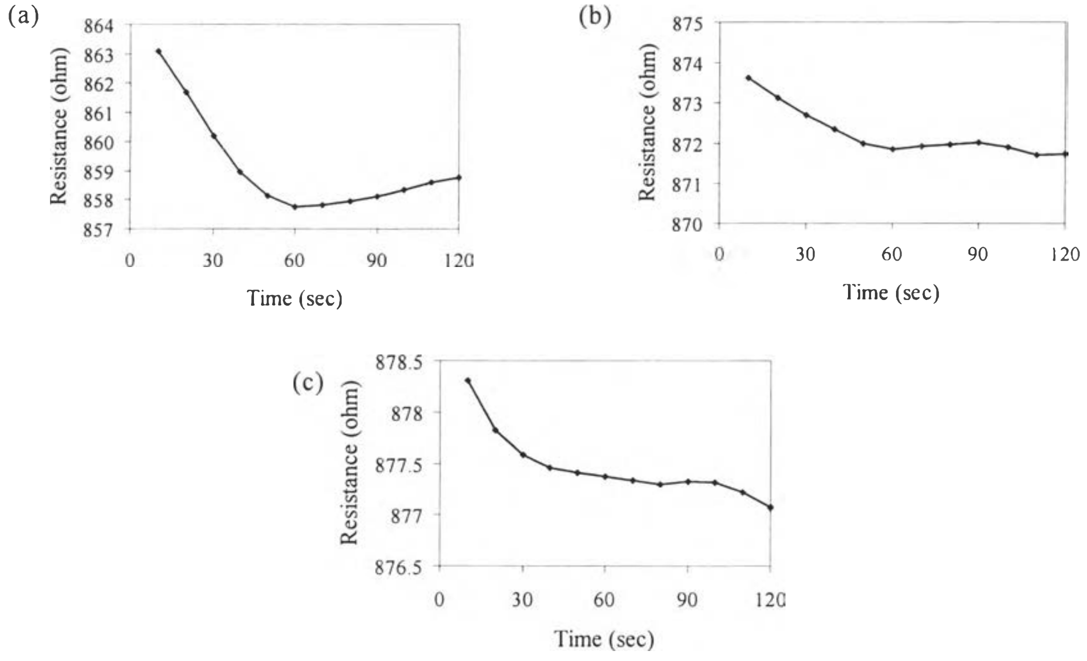

Figure G33 Resistance vs. time for PPy under CO_2:CH_4 at the ratio of (a) 1:1 (b) 1:2 and (c) 1:3.

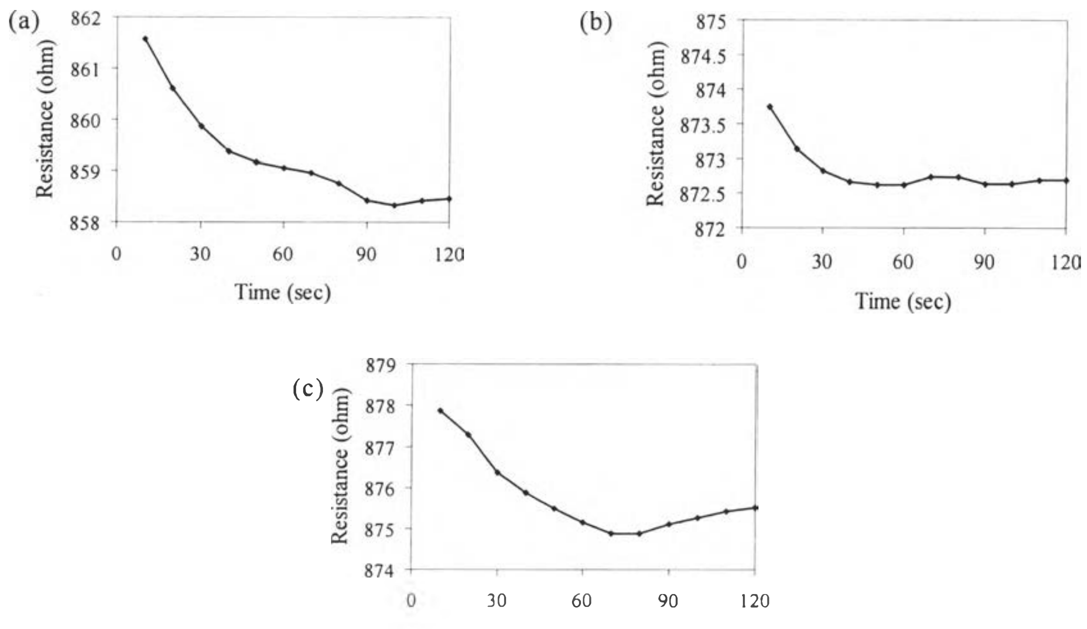

Figure G34 Resistance vs. time for PPyCl under CO_2:CH_4 at the ratio of (a) 1:1 (b) 1:2 and (c) 1:3.

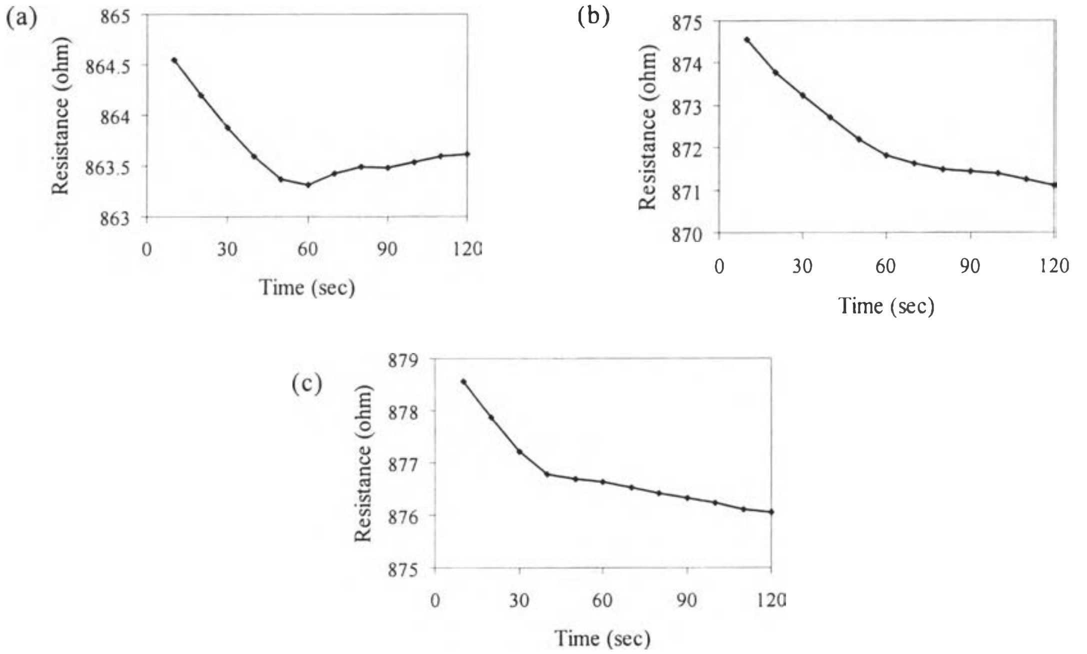

Figure G35 Resistance vs. time for PPyC3 under CO_2:CH_4 at the ratio of (a) 1:1 (b) 1:2 and (c) 1:3.

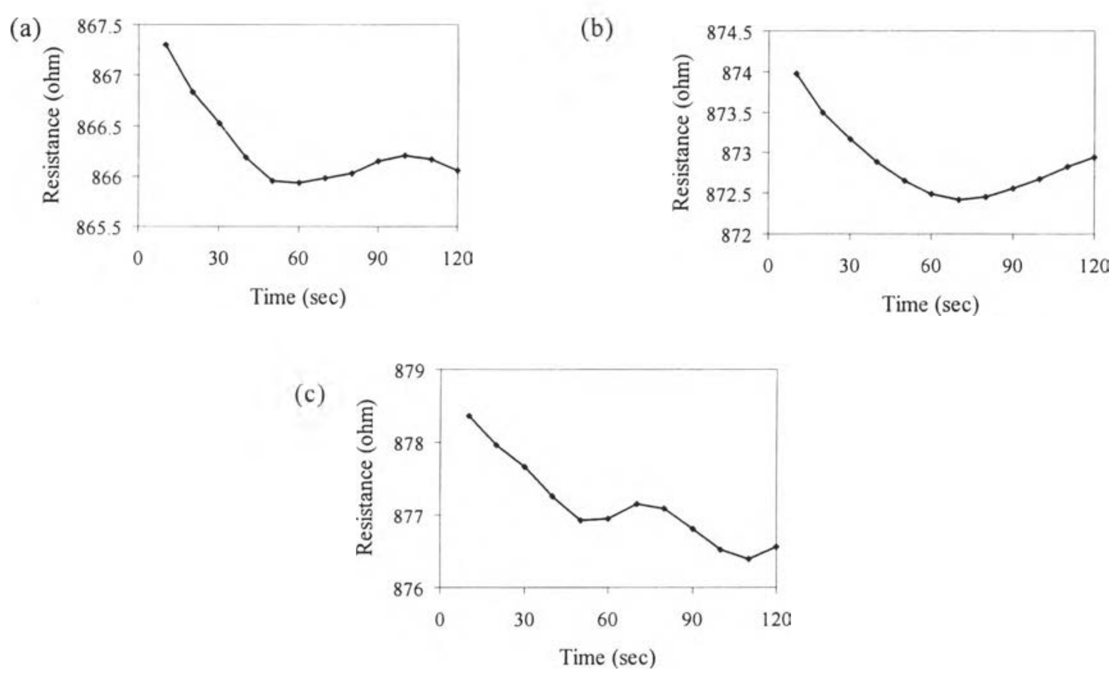

Figure G36 Resistance vs. time for PPyC6 under CO_2:CH_4 at the ratio of (a) 1:1 (b) 1:2 and (c) 1:3.

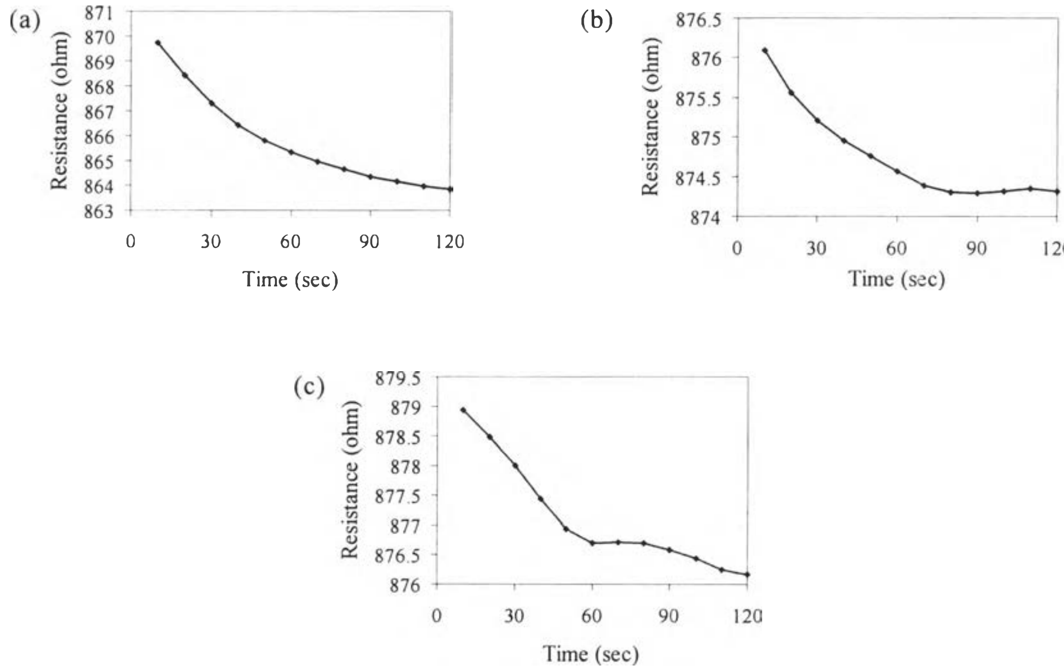

Figure G37 Resistance vs. time for PPyC9 under CO_2:CH_4 at the ratio of (a) 1:1 (b) 1:2 and (c) 1:3.

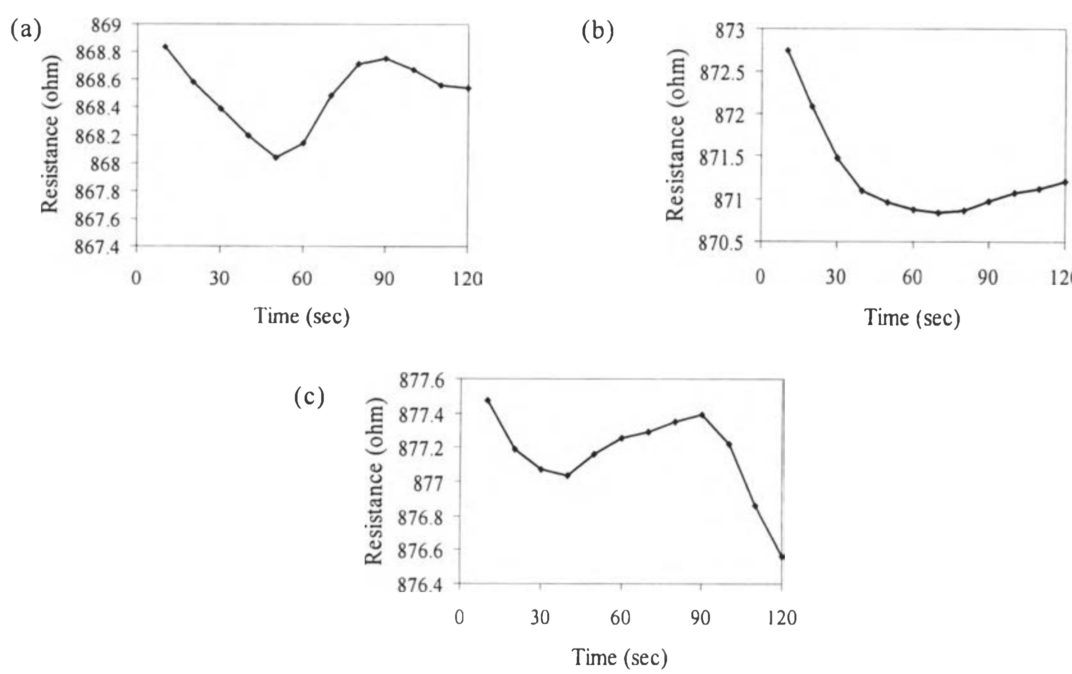

Figure G38 Resistance vs. time for DPPyC3 under CO_2:CH_4 at the ratio of (a) 1:1 (b) 1:2 and (c) 1:3.

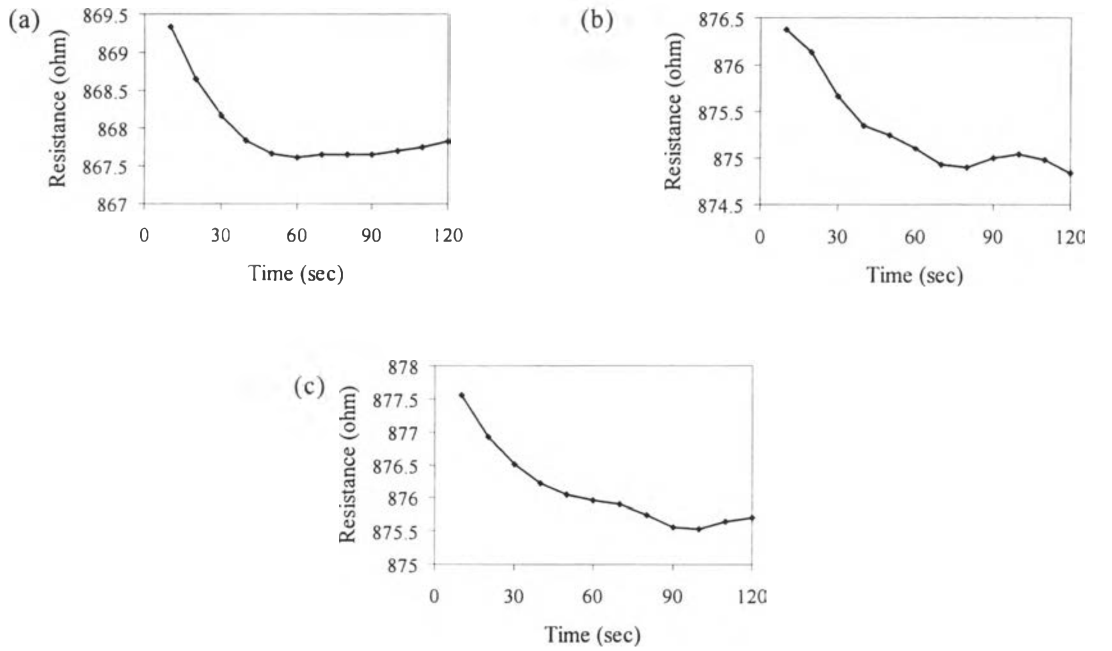

Figure G39 Resistance vs. time for nDPPyC3 under CO_2:CH_4 at the ratio of (a) 1:1 (b) 1:2 and (c) 1:3.

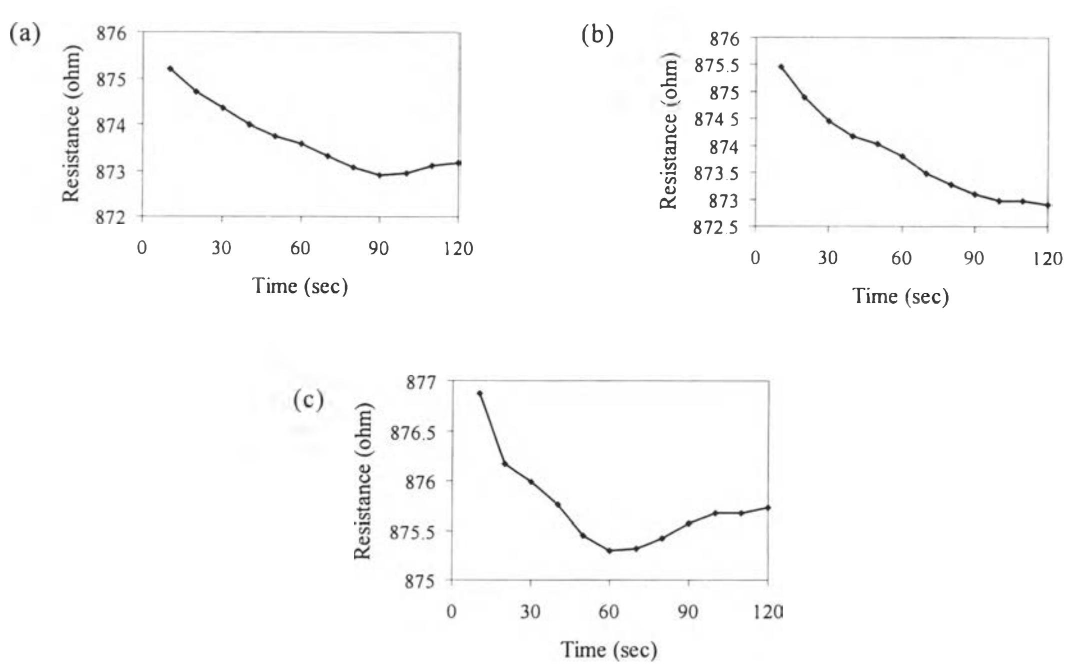

Figure G40 Resistance vs. time for PPy under CO_2:C_2H_4 at the ratio of (a) 1:1 (b) 1:2 and (c) 1:3.

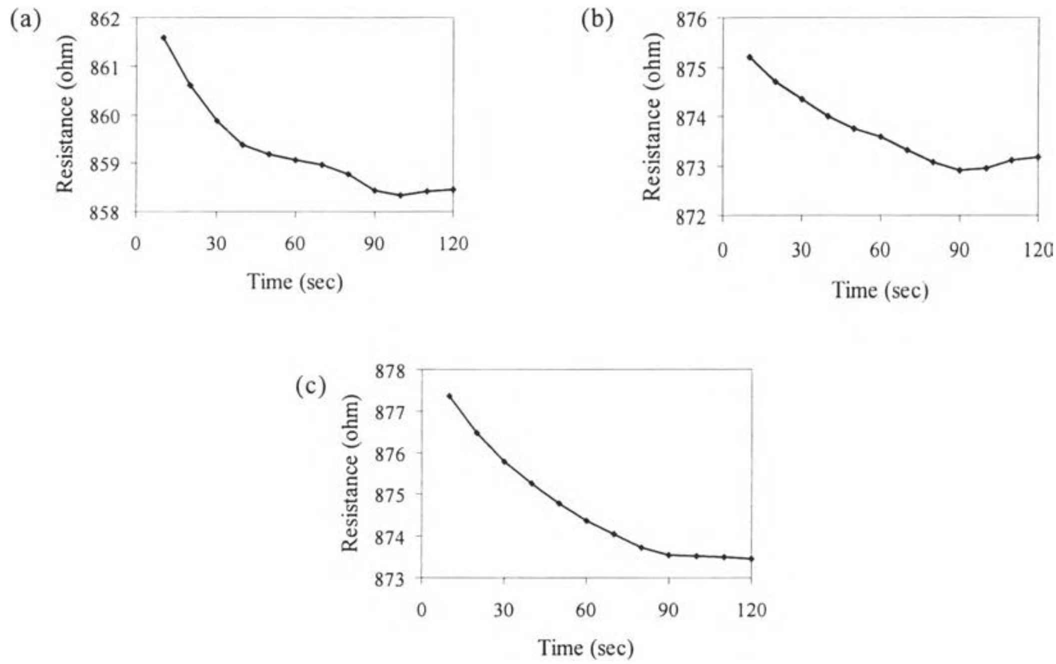

Figure G41 Resistance vs. time for PPyC1 under CO_2:C_2H_4 at the ratio of (a) 1:1 (b) 1:2 and (c) 1:3.

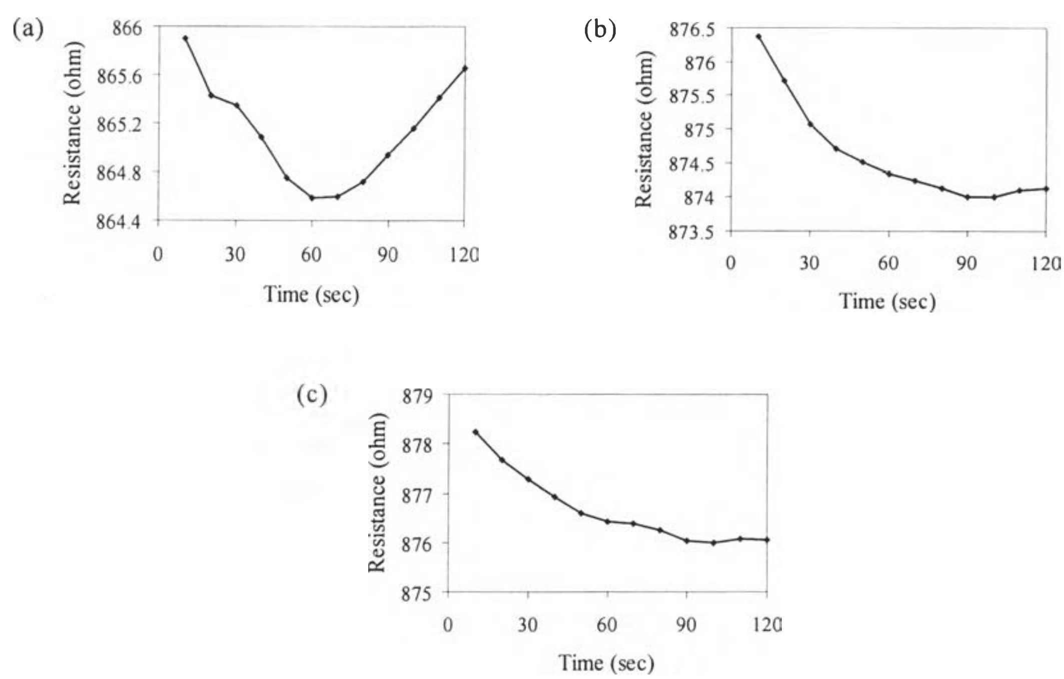

Figure G42 Resistance vs. time for PPyC3 under CO_2:C_2H_4 at the ratio of (a) 1:1 (b) 1:2 and (c) 1:3.

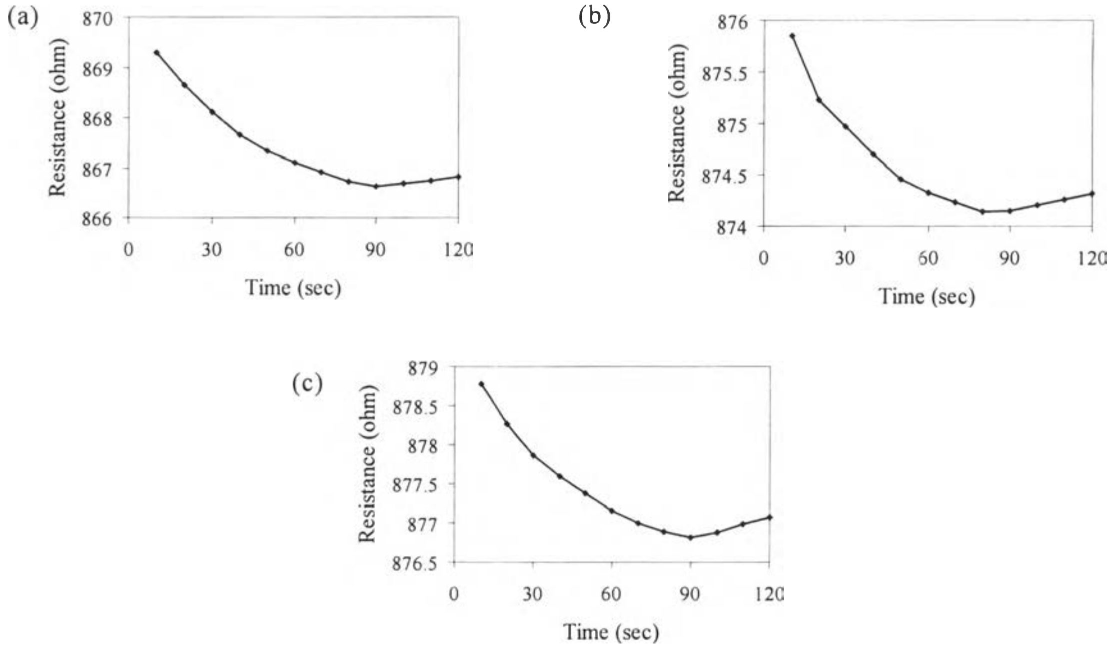

Figure G43 Resistance vs. time for PPyC6 under CO_2:C_2H_4 at the ratio of (a) 1:1 (b) 1:2 and (c) 1:3.

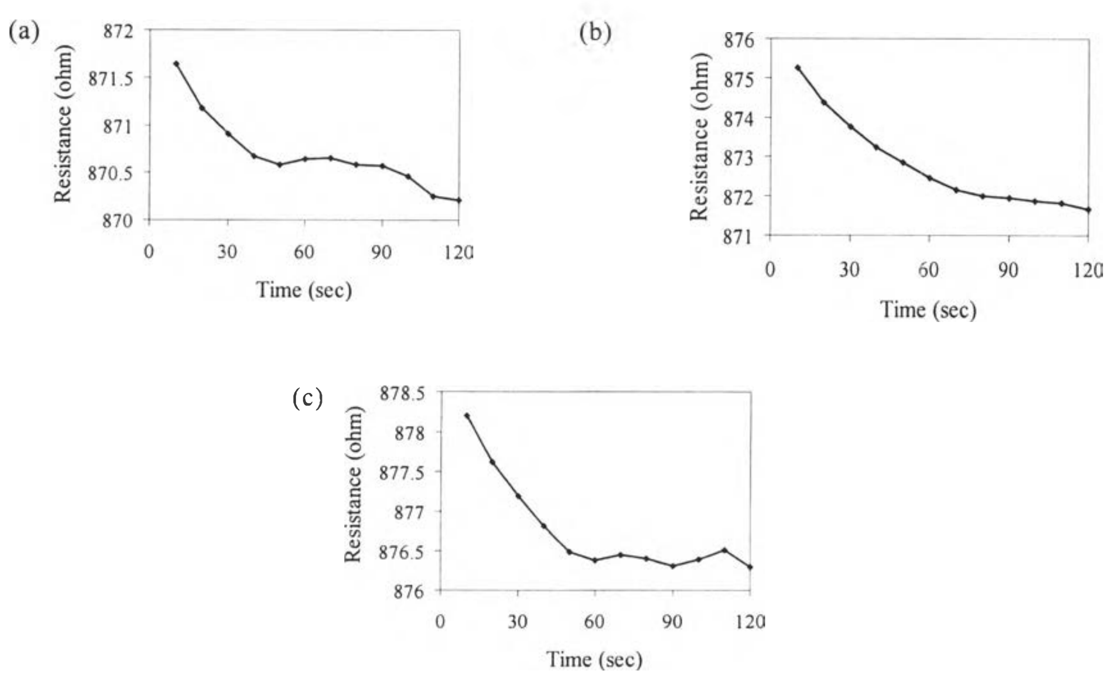

Figure G44 Resistance vs. time for PPyC9 under CO_2:C_2H_4 at the ratio of (a) 1:1 (b) 1:2 and (c) 1:3.

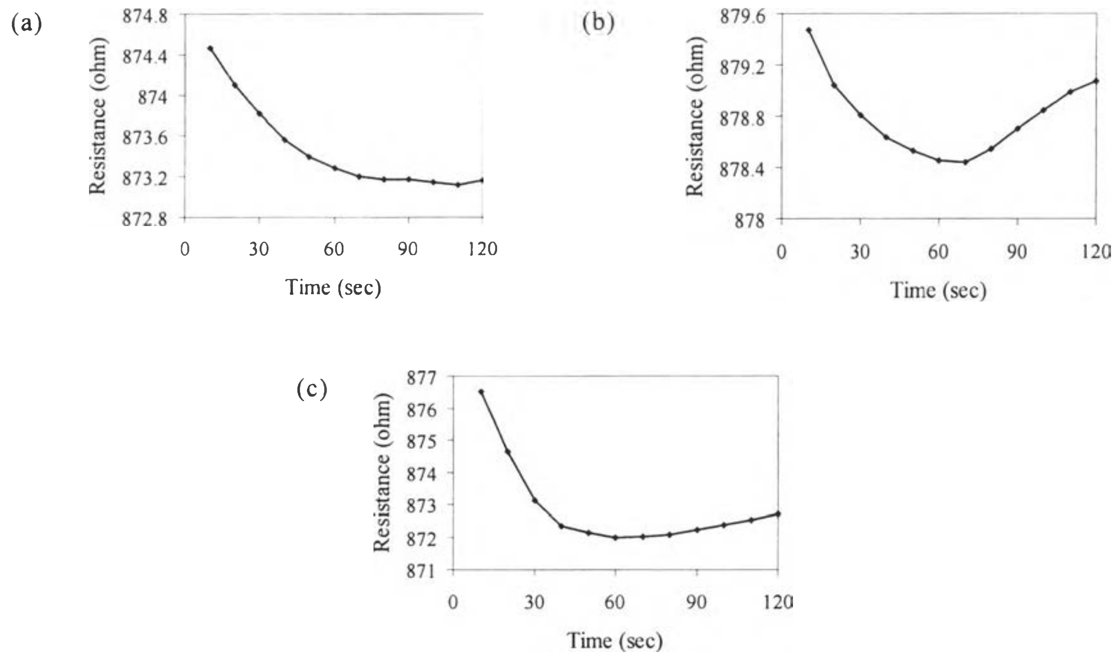

Figure G45 Resistance vs. time for DPPyC3 under CO_2:C_2H_4 at the ratio of (a) 1:1 (b) 1:2 and (c) 1:3.

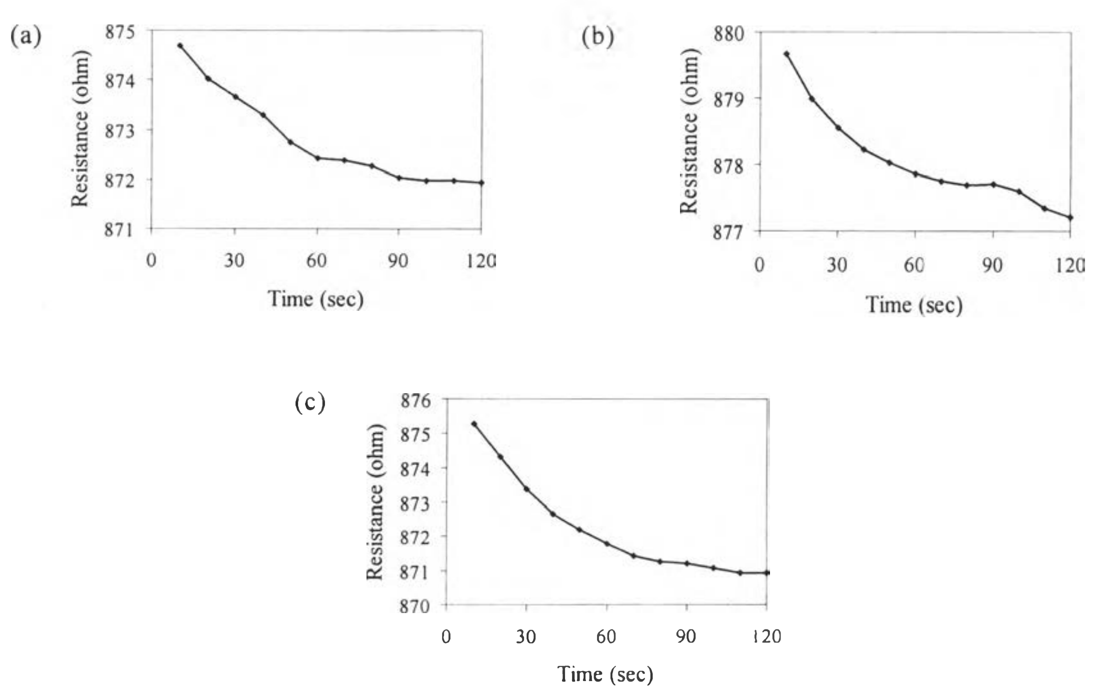

Figure G46 Resistance vs. time for nDPPyC3 under CO_2:C_2H_4 at the ratio of (a) 1:1 (b) 1:2 and (c) 1:3.

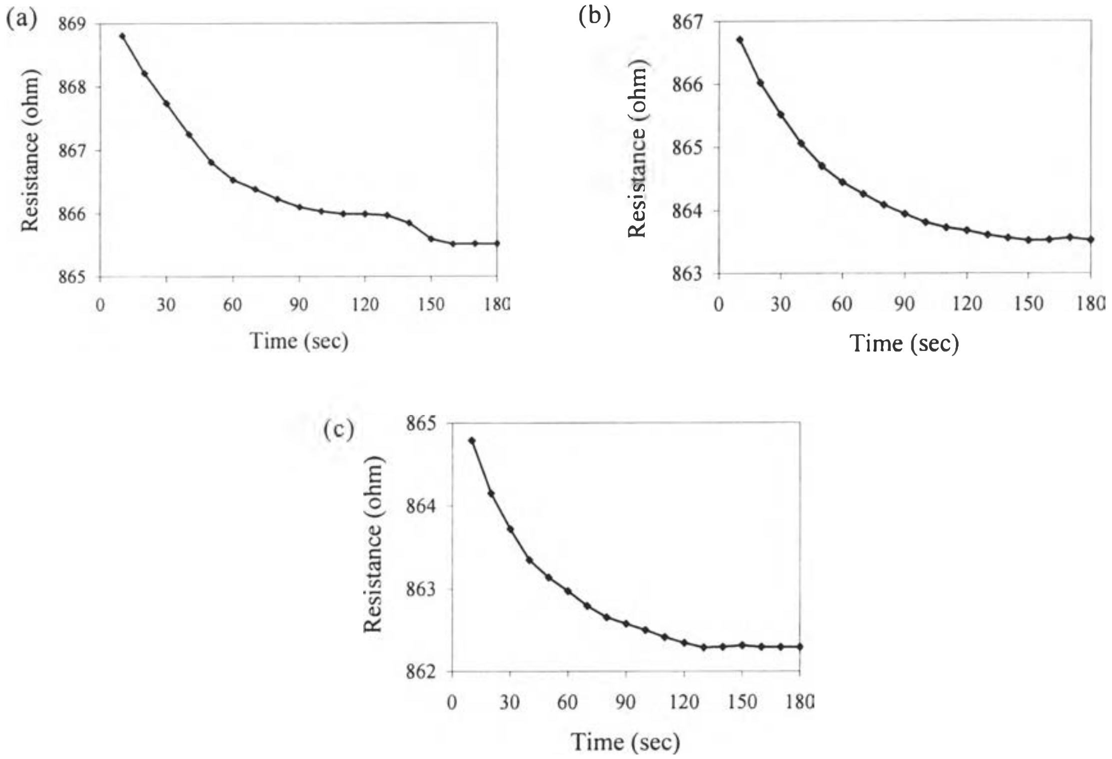

Figure G47 Resistance vs. time for nDPPyC3 of 0.5mm thick under (a) CO_2, (b) CH_4 and (c) C_2H_4 at the gas pressure of 0.1 bars.

Appendix H Characterization of nDPPyC3

nDPPyC3 was characterized by FTIR, XRD, and TGA as shown in Figure H1.

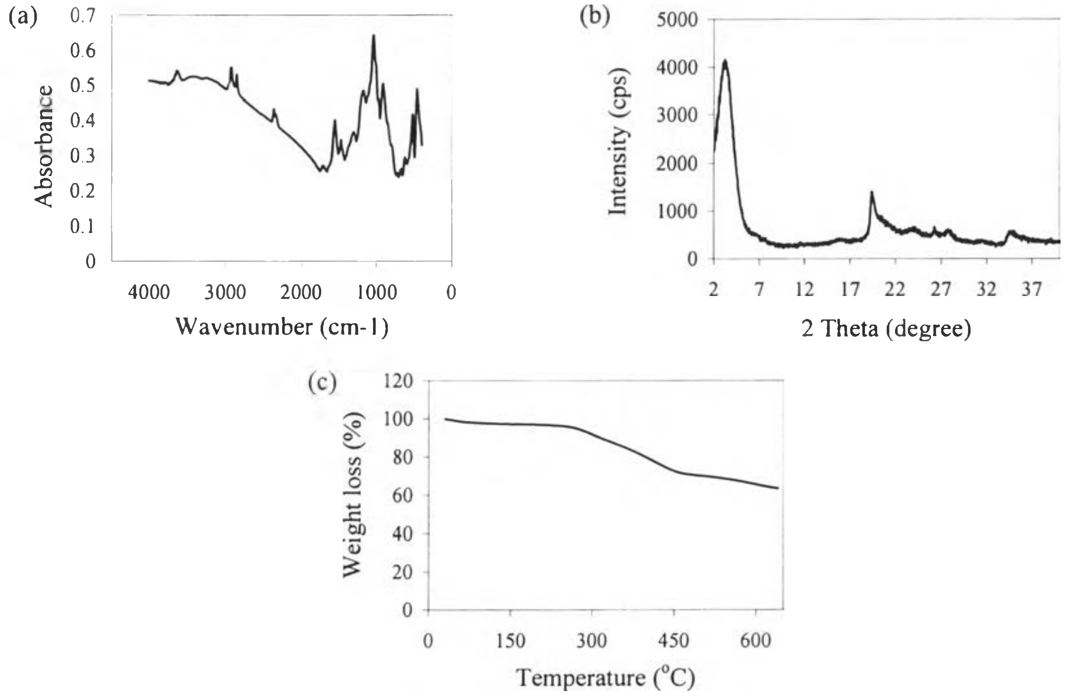

Figure H1 (a) A FTIR spectrum, (b) An XRD pattern, and (c) A TGA curve under O_2 atmosphere for nDPPyC3.

The results of nDPPyC3 obtained from these following tests (see Figure H1) were corresponded to the results of DPPyC3, indicating that nDPPyC3 was still the nanocomposites containing intercalated OC-MMT and exfoliated Na-MMT.

CURRICULUM VITAE

Name: Ms. Acharaporn Thuimthad

Date of Birth: December 06, 1979

Nationality: Thai

University Education:

1998-2002 Bachelor's Degree of Science in Chemistry, Faculty of science, Chulalongkorn University, Bangkok, Thailand.

Presentation:

1. Poster presentation, "Preparation and Characterization of Polypyrrole-Layered Silicate Nanocomposites", at the 8^{th} Pacific Polymer Conference, November 24^{th}-27^{th}, 2003, Bangkok, Thailand.